Status of the Ricochet experiment

Valentina Novati

seminar at USTC
August 20th, 2025 - Hefei

The Ricochet collaboration

RICOCHET
A Coherent Neutrino Scattering Program

Outline

- Coherent elastic neutrino nucleus scattering
- The Ricochet experiment
- Commissioning results

Outline

- Coherent elastic neutrino nucleus scattering
- The Ricochet experiment
- Commissioning results

Coherent elastic neutrino-nucleus scattering

The coherent elastic neutrino-nucleus scattering (CEνNS) proposed by Freedman in 1974

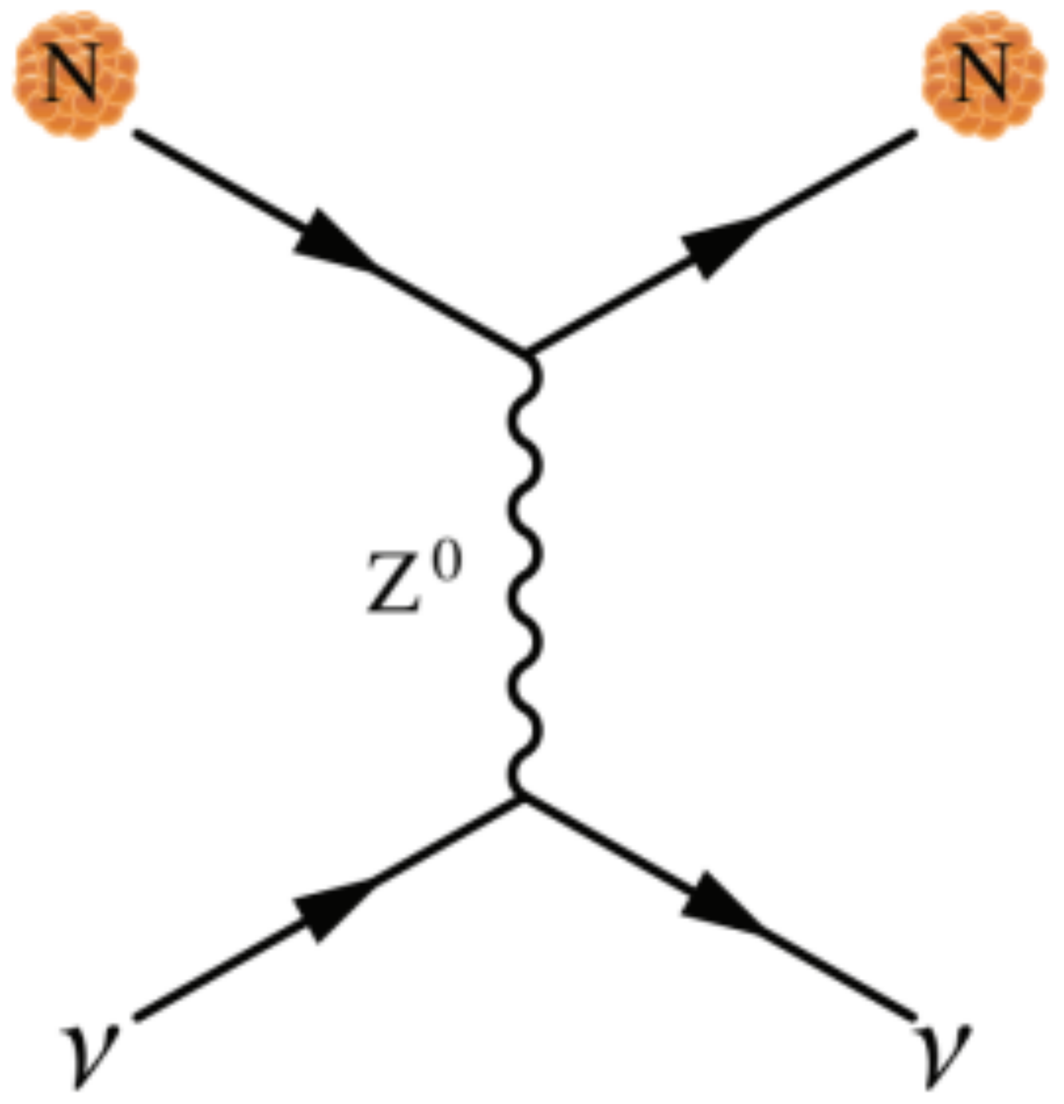

PHYSICAL REVIEW D VOLUME 9, NUMBER 5 1 MARCH 1974

Coherent effects of a weak neutral current

Daniel Z. Freedman†
National Accelerator Laboratory, Batavia, Illinois 60510
and Institute for Theoretical Physics, State University of New York, Stony Brook, New York 11790
(Received 15 October 1973; revised manuscript received 19 November 1973)

If there is a weak neutral current, then the elastic scattering process $\nu + A \to \nu + A$ should have a sharp coherent forward peak just as $e + A \to e + A$ does. Experiments to observe this peak can give important information on the isospin structure of the neutral current. The experiments are very difficult, although the estimated cross sections (about 10^{-38} cm^2 on carbon) are favorable. The coherent cross sections (in contrast to incoherent) are almost energy-independent. Therefore, energies as low as 100 MeV may be suitable. Quasi-coherent nuclear excitation processes $\nu + A \to \nu + A^*$ provide possible tests of the conservation of the weak neutral current. Because of strong coherent effects at very low energies, the nuclear elastic scattering process may be important in inhibiting cooling by neutrino emission in stellar collapse and neutron stars.

D. Z. Freedman, Phys. Rev. D 9, 1389 (1974)

CEvNS

Detector targets with large M_A are preferable

F~1 for low momentum neutrinos (i.e. reactor neutrinos)

$$\frac{d\sigma}{dT} = \frac{G_F^2}{4\pi} Q_W^2 M_A \left(1 - \frac{M_A T}{2E_\nu^2}\right) F(q^2)^2$$

- σ → cross section
- T → Recoil energy
- E → neutrino energy
- G_F → Fermi constant
- Q_W → weak charge, related to sin(W)
- M_A → atomic mass
- F → form factor

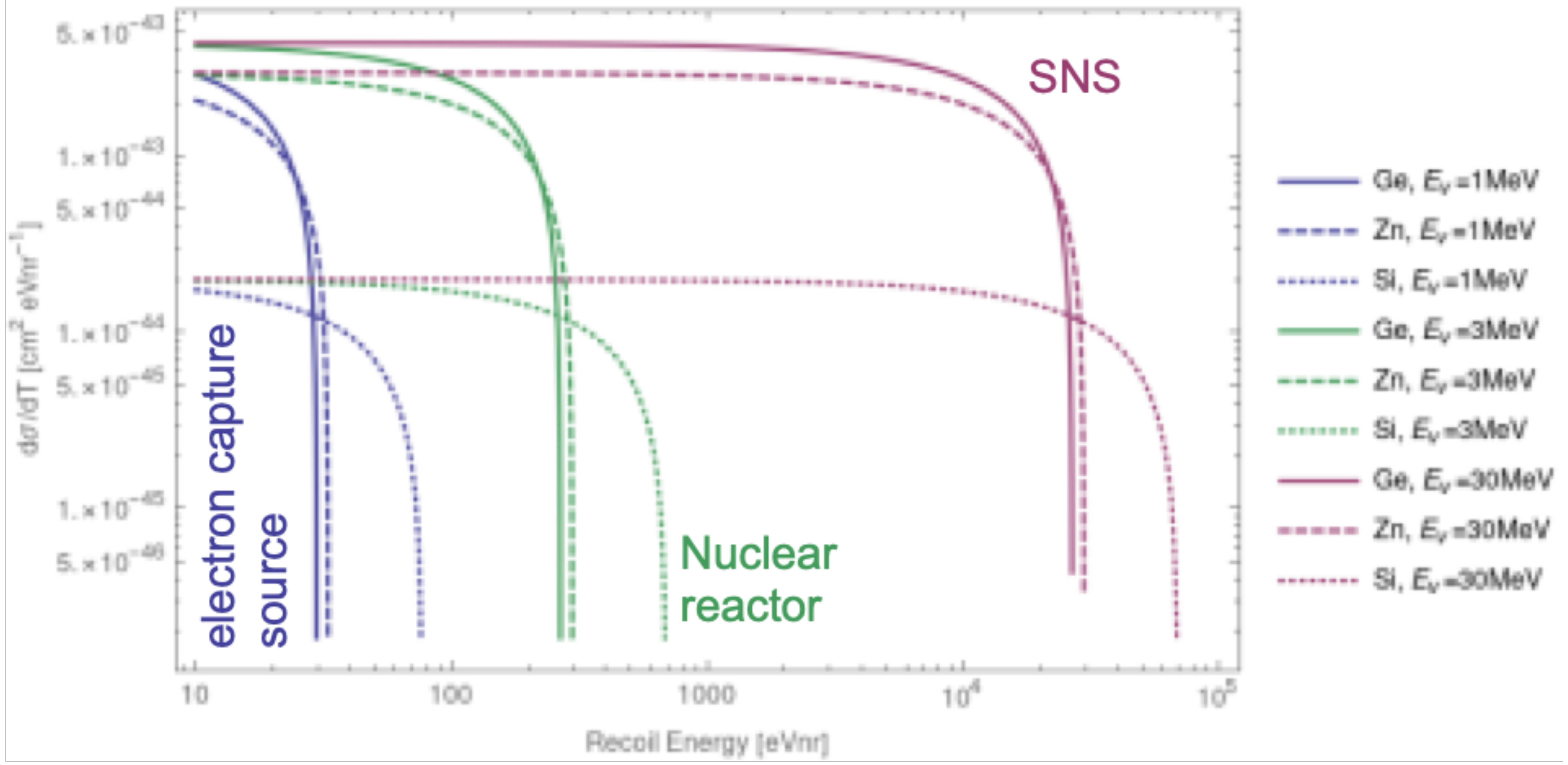

No flavour-specific term, same rate for ν_e, ν_μ and ν_τ

First detections from COHERENT

First detection of CEvNS occurred 43 years after Freedman article

The COHERENT experiment measured it with sodium-doped CsI at the SNS for the first time

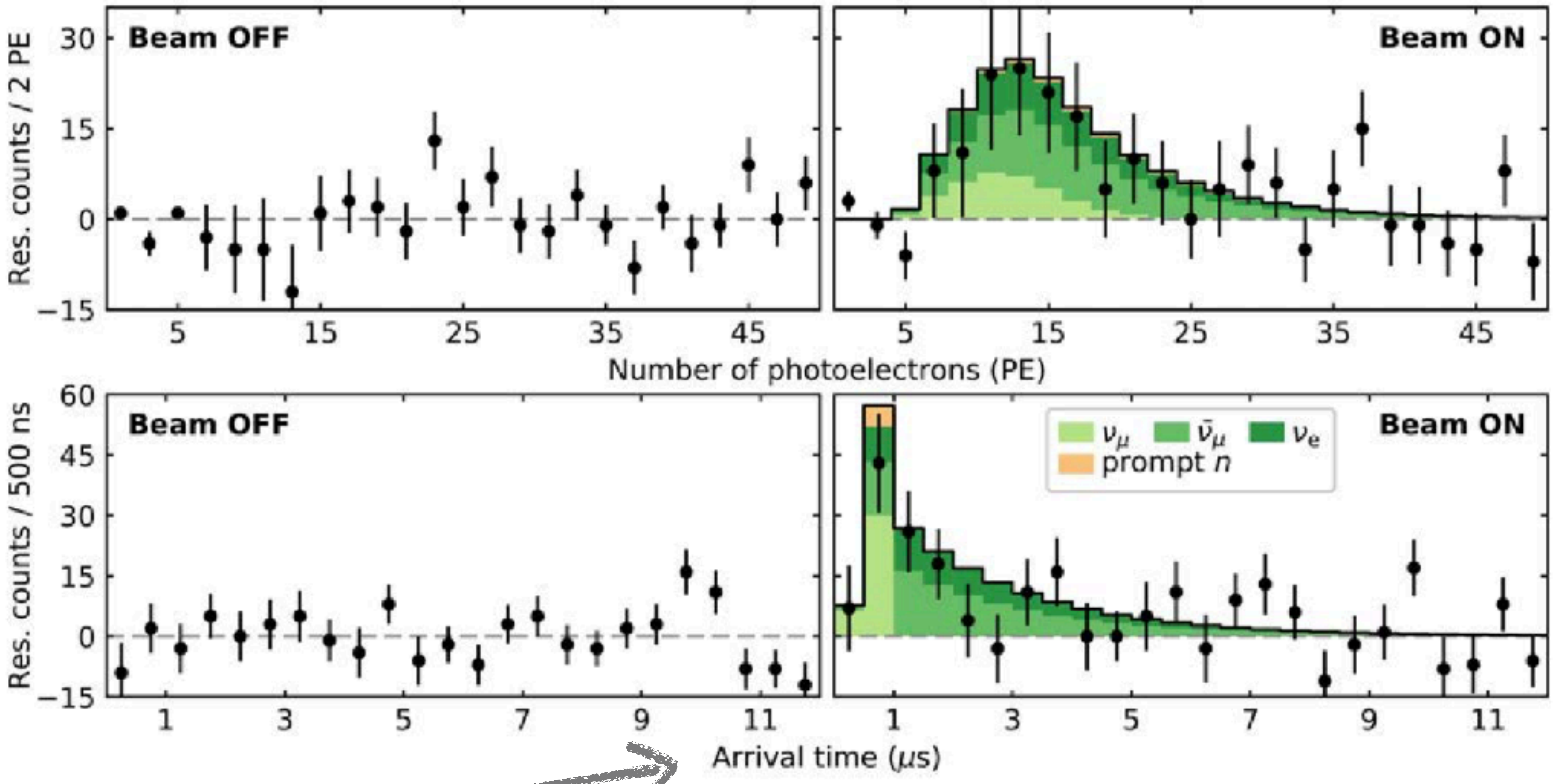

The SNS is a pulsed source

D. Akimov et al., Science 357, 1123, (2017) - ArXiv:1708.01294

First detections from COHERENT

From 2017, the COHERENT Collaboration measured it with different targets at the SNS:

- sodium-doped CsI
- argon
- germanium

Credit M.P. Green MAG7s 2025

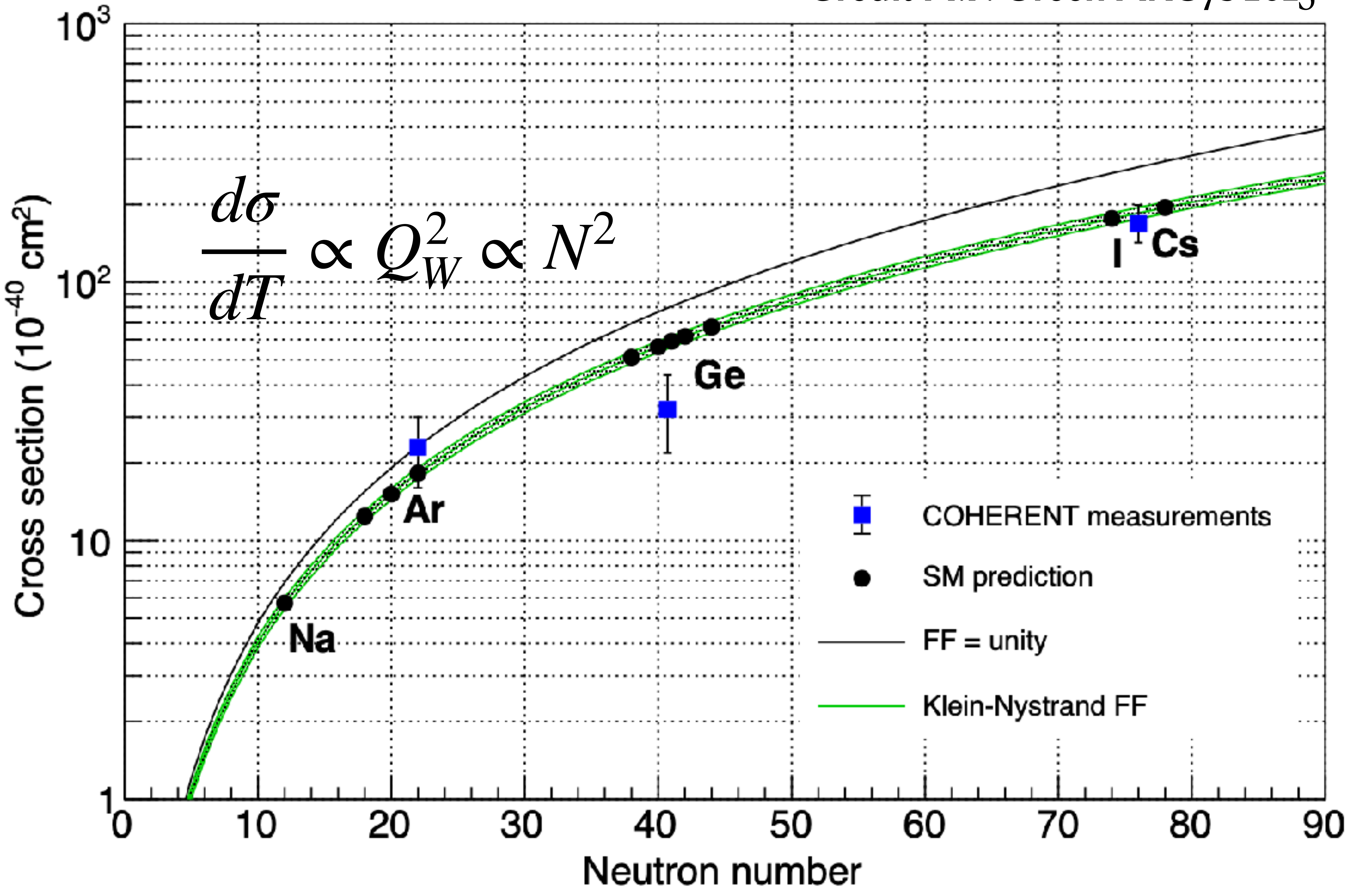

PRL 129, 081801 (2022) - arXiv:2110.07730
PRL 126 012002 (2021) - arXiv:2003.10630
PRL 134, 231801 (2025) - arXiv:2406.13806

Experiments

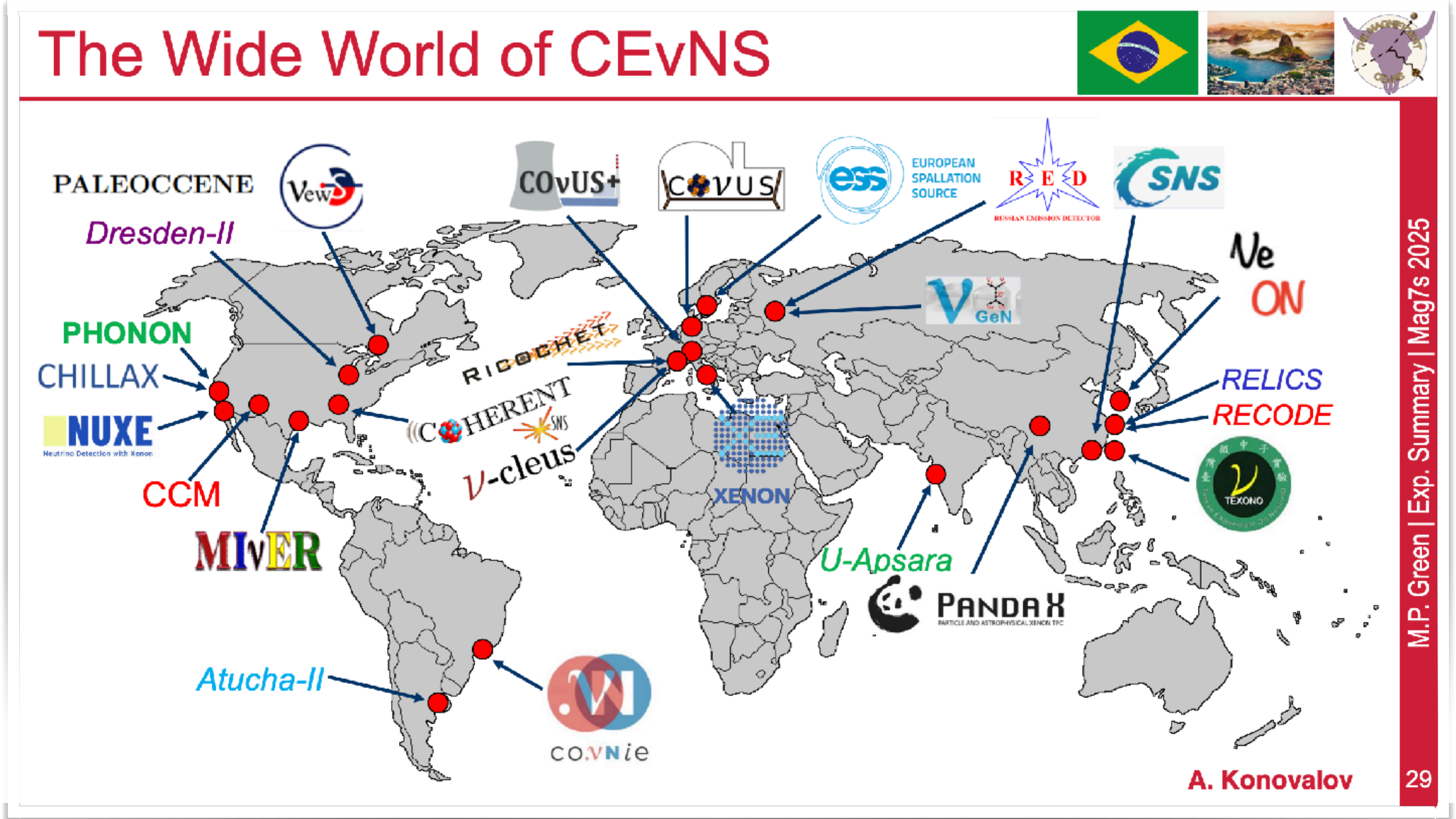

A probe for physics beyond the Standard Model

$$\frac{d\sigma}{dT} = \frac{G_F^2}{4\pi} Q_W^2 M_A \left(1 - \frac{M_A T}{2E_\nu^2}\right) F(q^2)^2$$

Q_W → weak charge

$$Q_W = N - Z(1 - 4sin^2\theta_W)$$

Weinberg angle

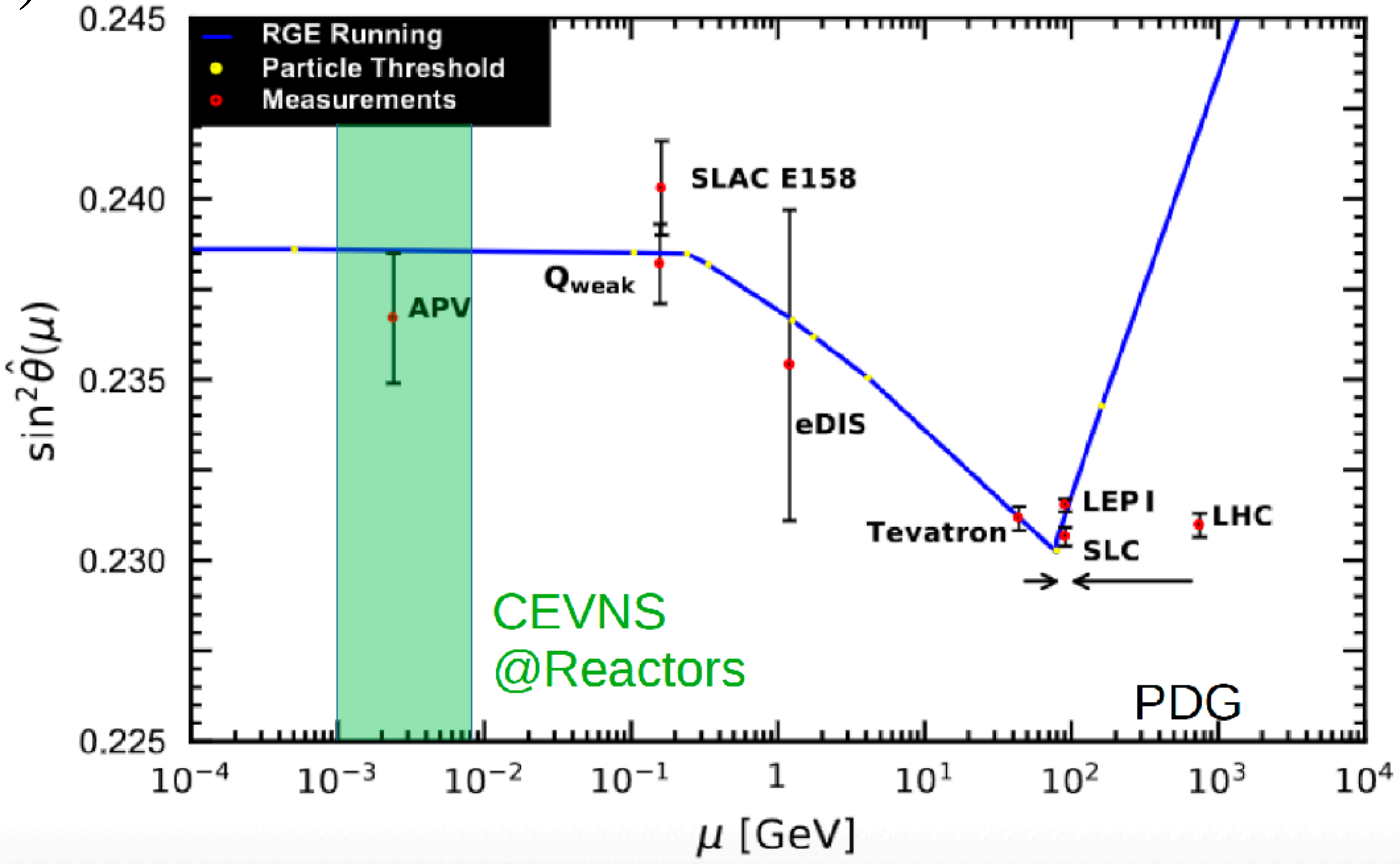

A probe for physics beyond the Standard Model

Test for physics beyond the Standard Model:

- non-standard interactions of neutrinos and quarks
- neutrino magnetic moment
- neutrino couplings to new mediators
- sterile neutrinos

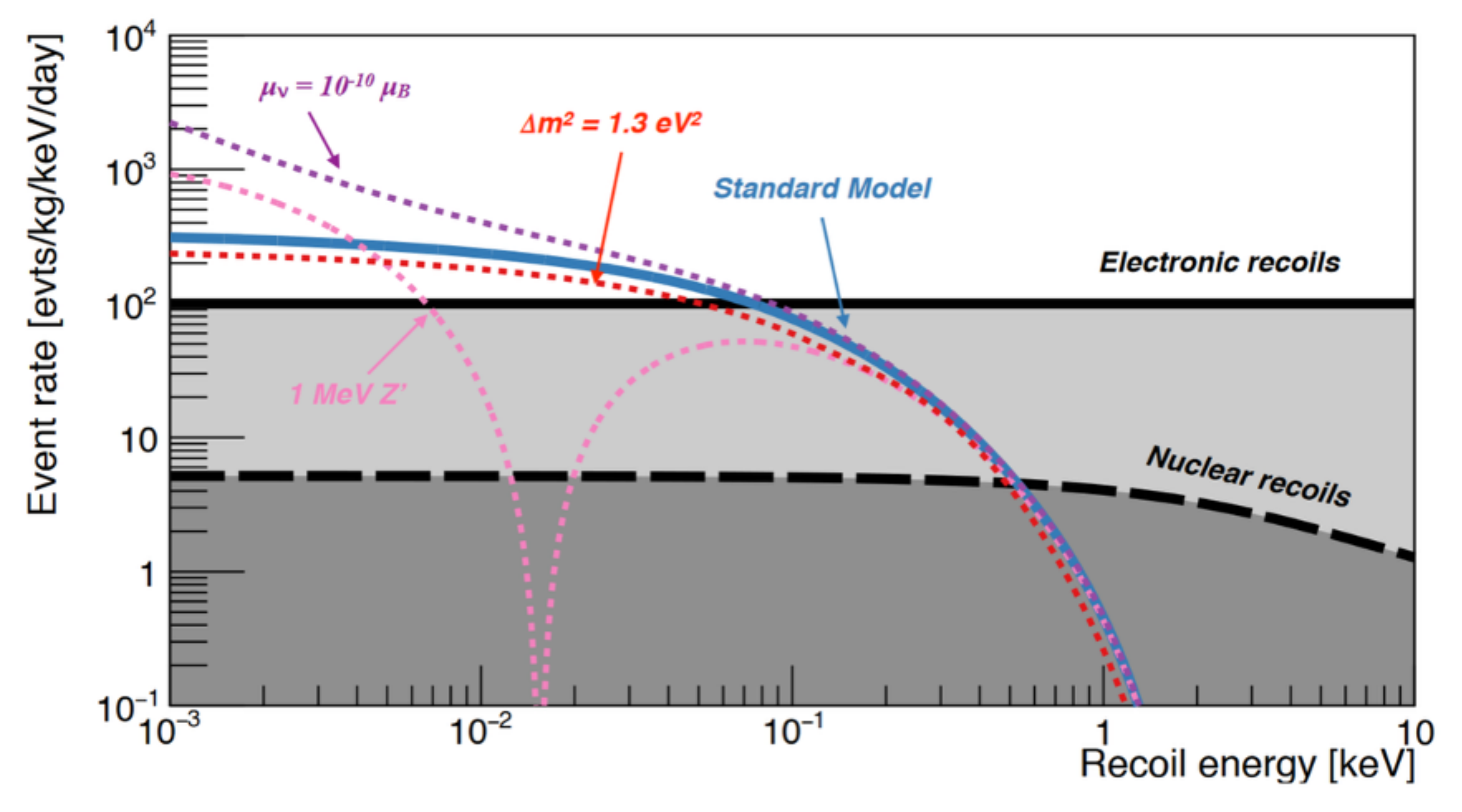

Need large exposure to be sensitive to physics beyond the Standard Model

Reactor antineutrinos

- Reactors are a source of antineutrinos with a larger flux than the SNS
- Lower neutrino energy

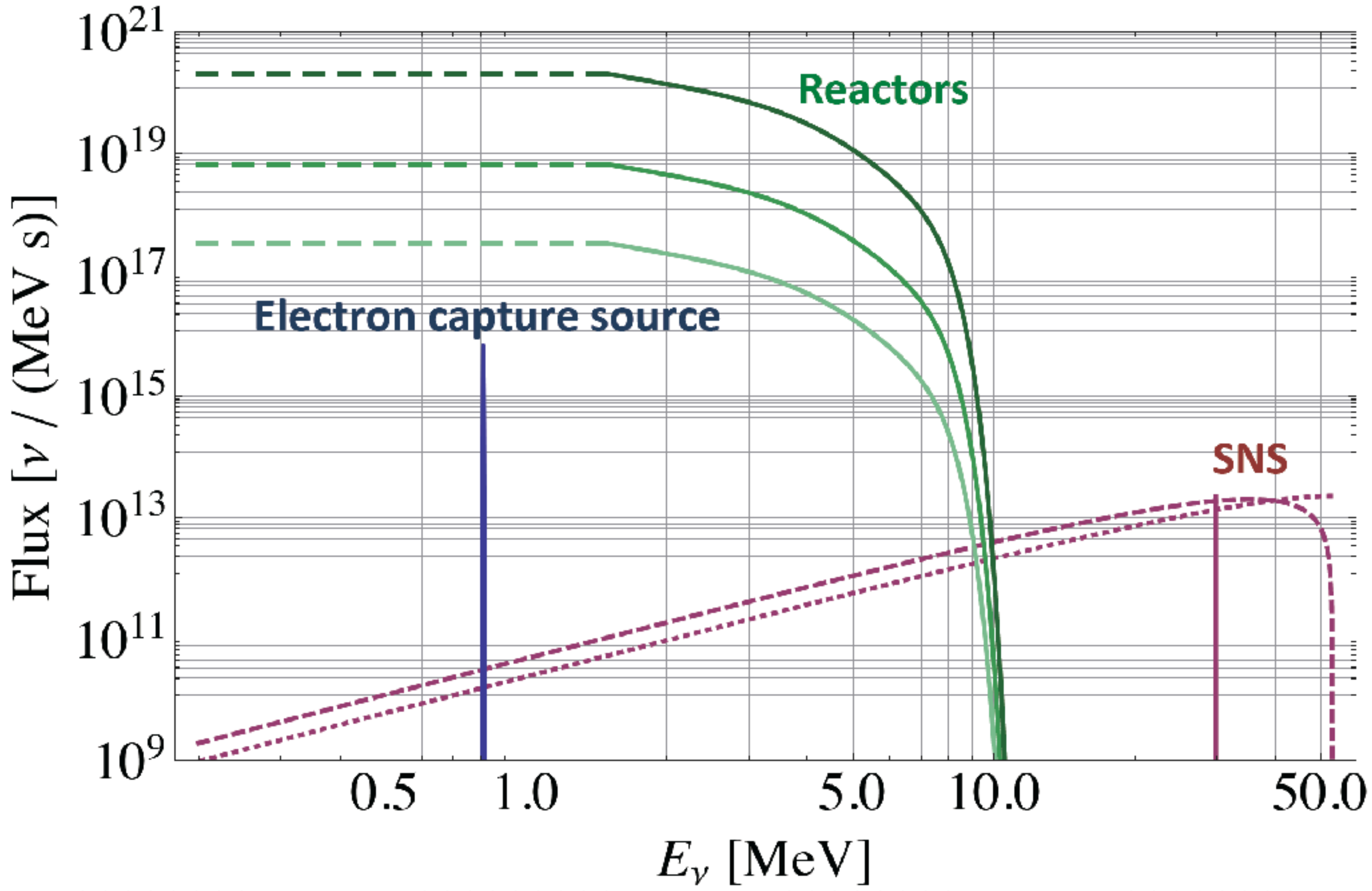

Despite the high antineutrino flux, the interactions are still rare

Detectors with a low-energy threshold are required

Reactor antineutrinos

- Reactors are a source of antineutrinos with a larger flux than the SNS
- Lower neutrino energy

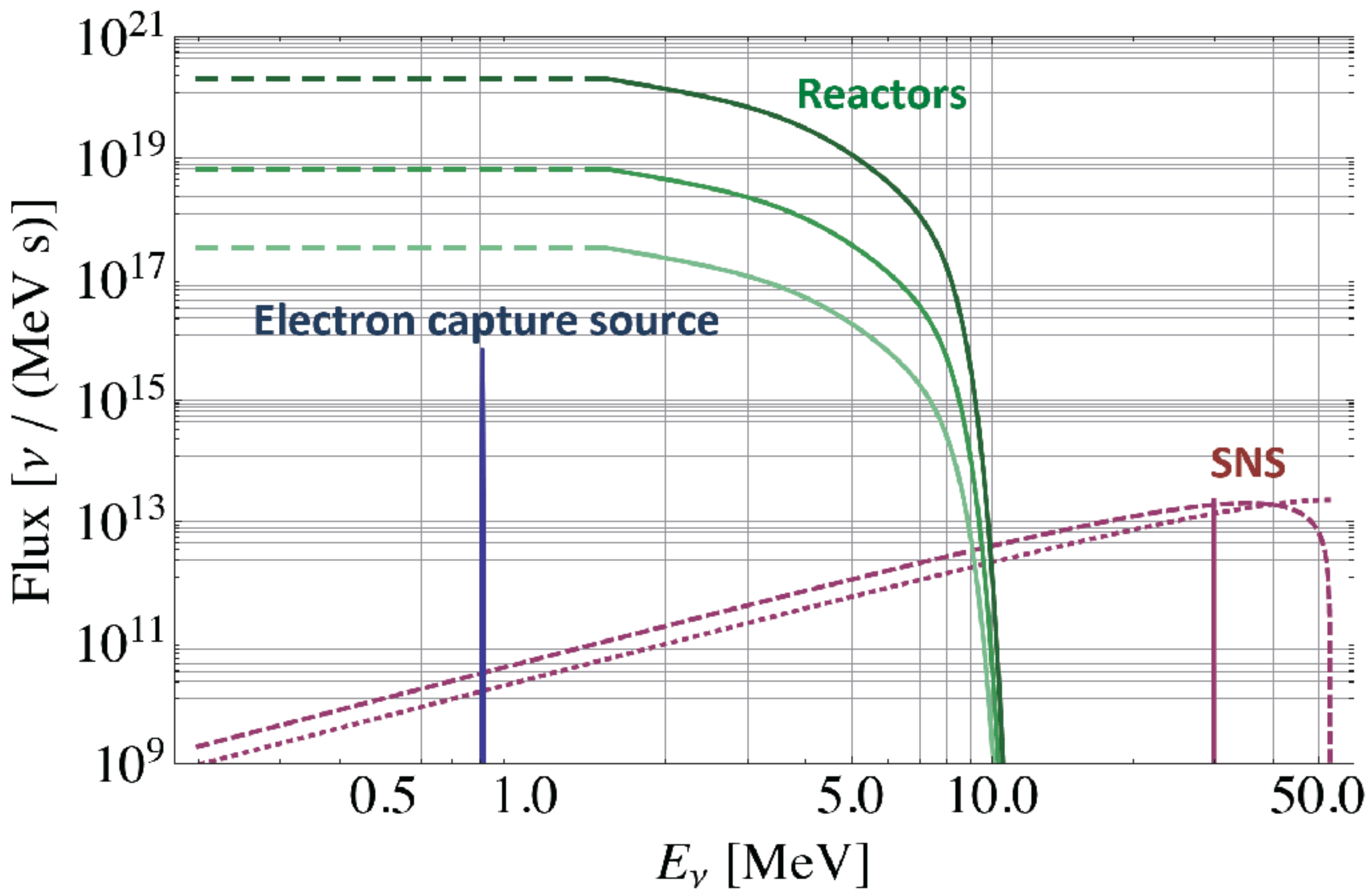

Solid-state detectors are good candidates, **semiconductor** targets are a common choice

Detectors with a low-energy threshold are required

Caveat: ionization yield quenching

- Neutrinos interact with the nucleus
  → nuclear recoil event
- Nuclear recoils produce less ionization than electron recoils in semiconductors
  → ionization yield quenching

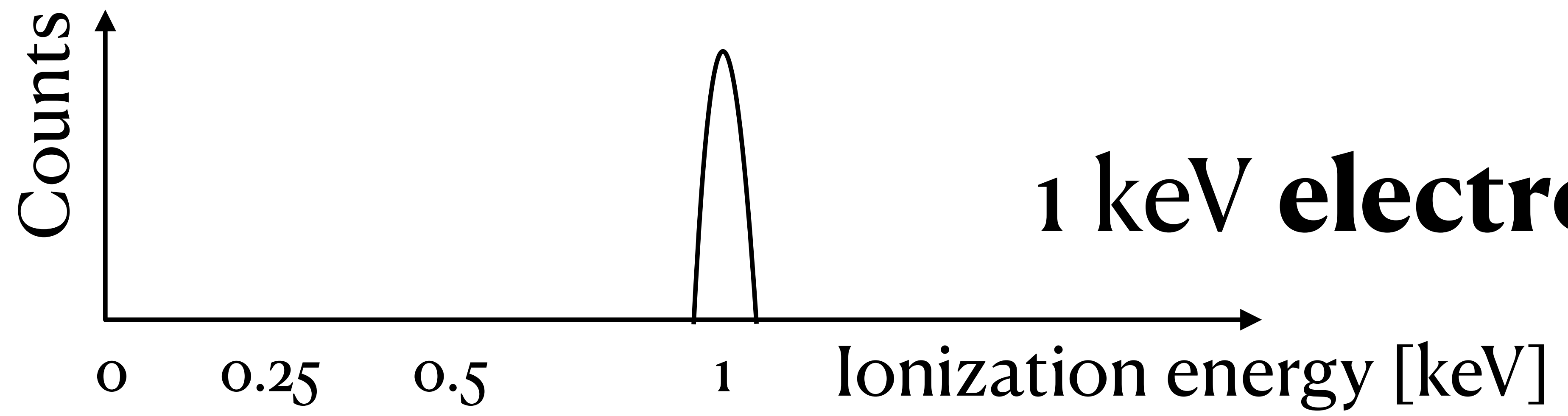

1 keV **electron** recoil

1 keV **nuclear** recoil

Lindhard theoretical model published in 1963

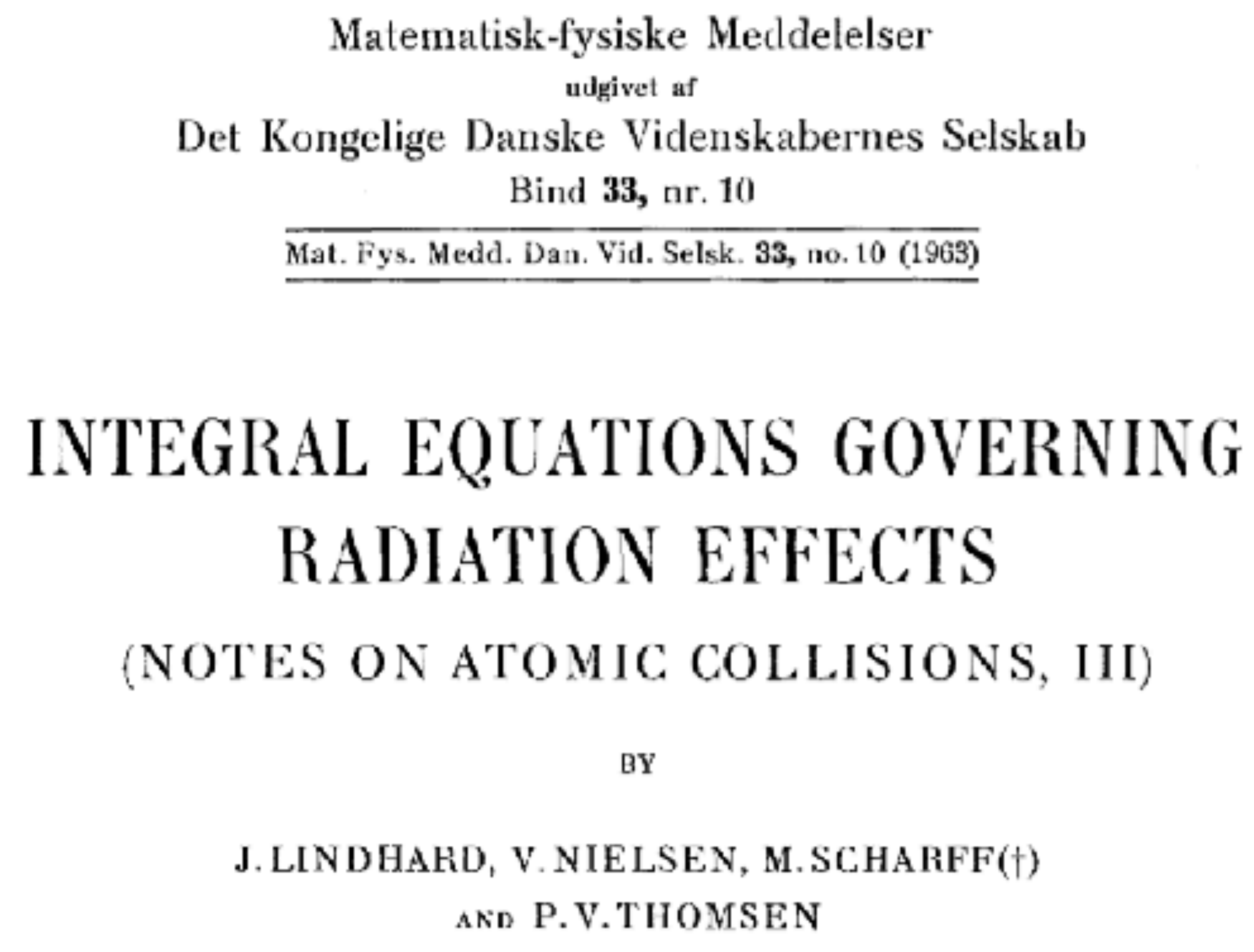

Matematisk-fysiske Meddelelser
udgivet af
Det Kongelige Danske Videnskabernes Selskab
Bind **33**, nr. 10

Mat. Fys. Medd. Dan. Vid. Selsk. **33**, no. 10 (1963)

INTEGRAL EQUATIONS GOVERNING RADIATION EFFECTS

(NOTES ON ATOMIC COLLISIONS, III)

BY

J. LINDHARD, V. NIELSEN, M. SCHARFF(†) AND P. V. THOMSEN

J. Lindhard, et al., Mat. Fys. Medd. Dan . Vid. Selsk . 33, no . 10 (1963)

Caveat: ionization yield quenching

Quenching factor (%)

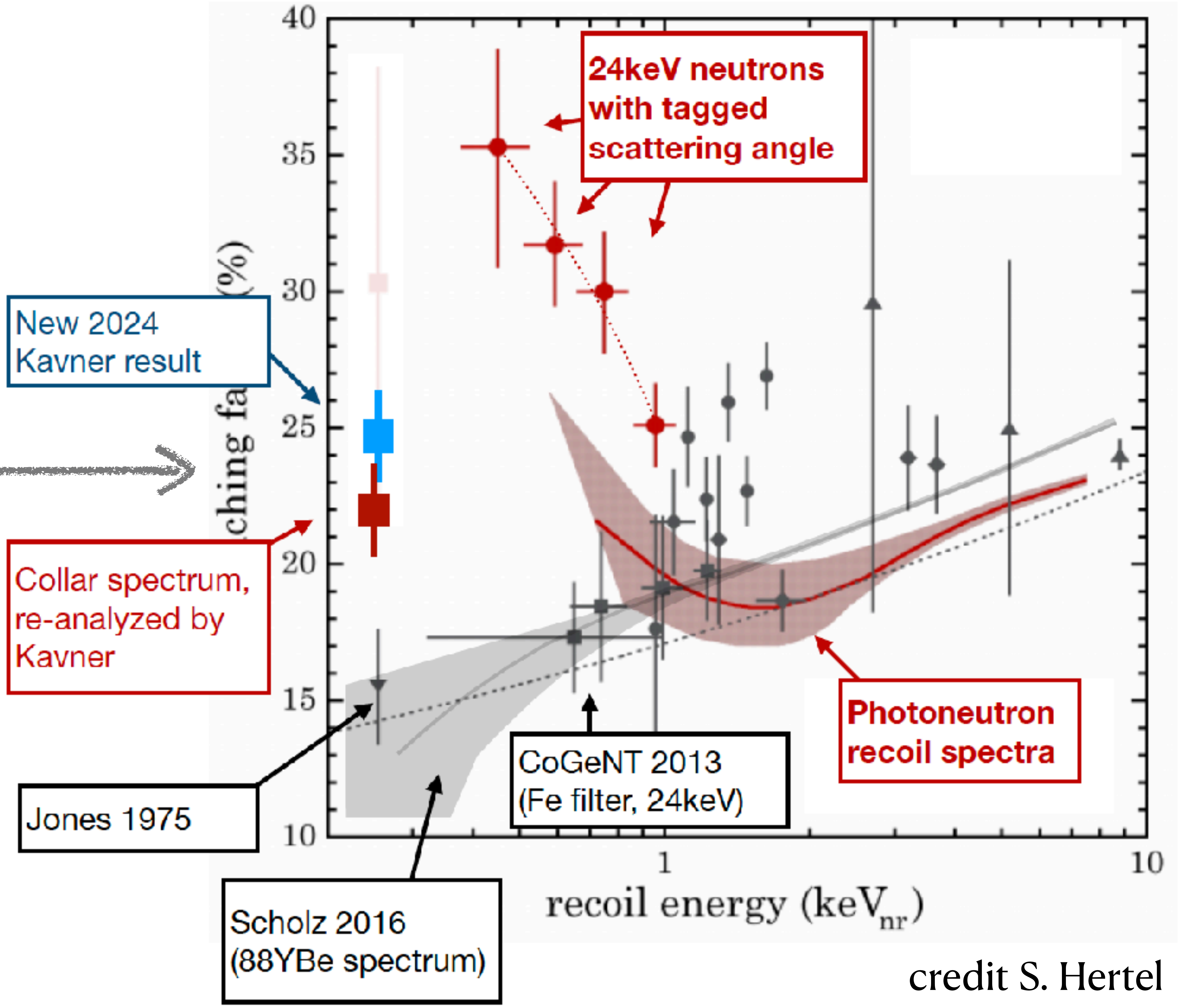

credit S. Hertel

Dresden II

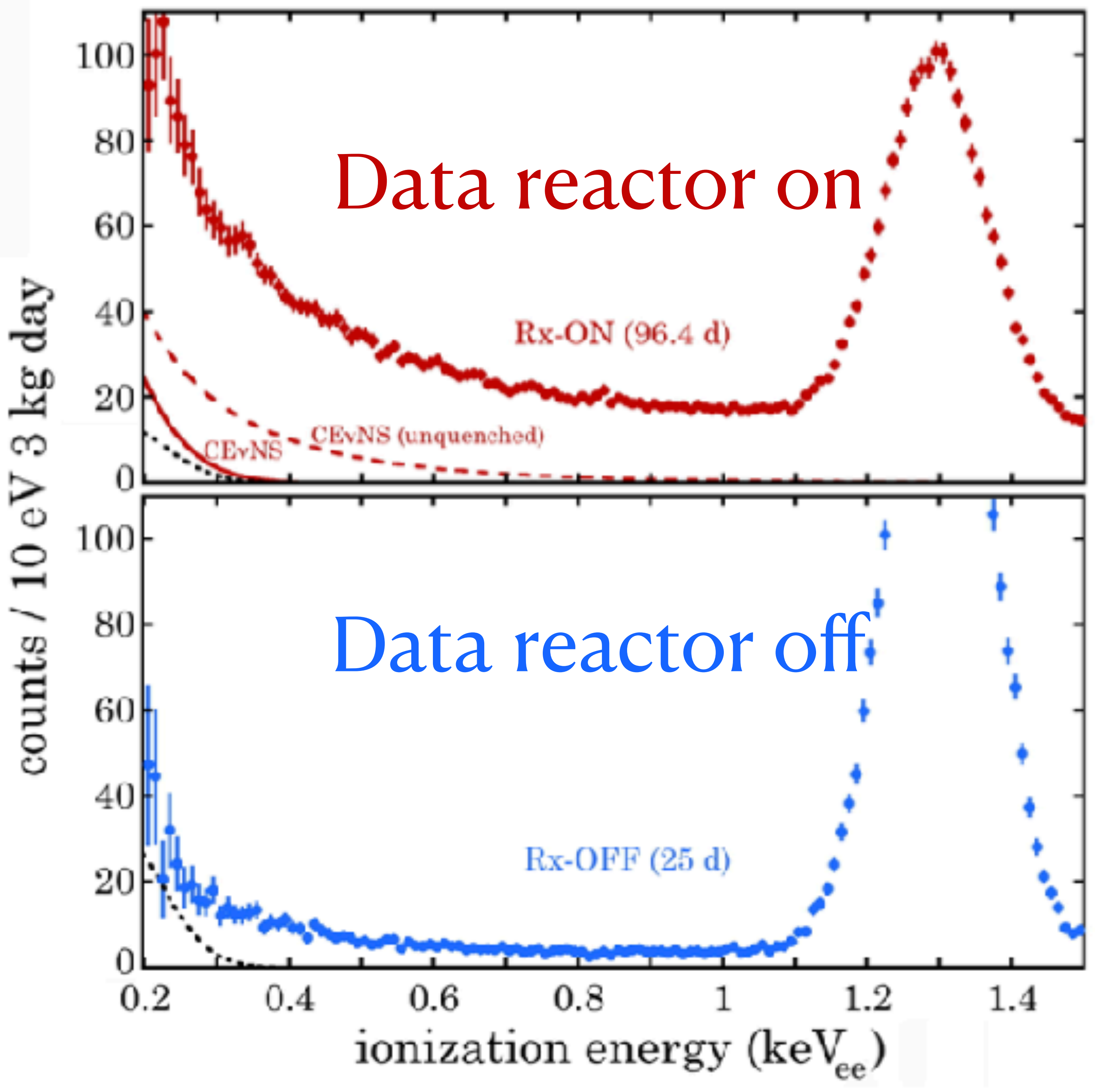

FIG. 1. Energy spectra of PPC bulk events during Rx-ON and Rx-OFF periods. The CEνNS expectation (red line) uses the MHVE antineutrino spectrum and Fe-filter quenching factor (see text). A dashed red line illustrates the impact of quenching on CEνNS. Black dotted lines signal the ^{71}Ge M-shell EC contribution, derived from L-shell EC at 1.29 keV$_{ee}$. This process is noticeable in Rx-OFF data, taken prior to the addition of neutron moderator (i.e., following intense ^{71}Ge activation).

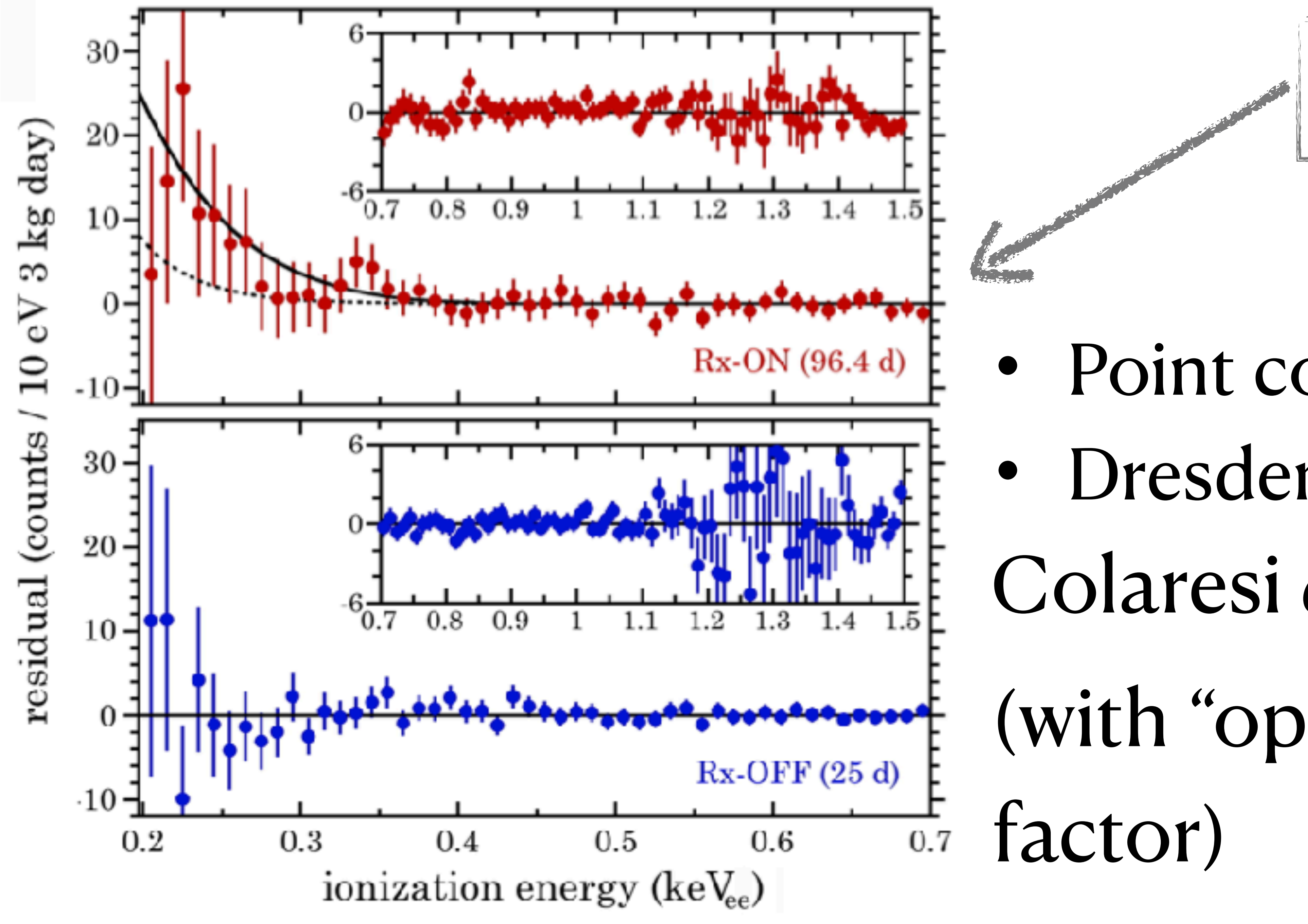

FIG. 5. Residual difference between the spectra of Fig. 1 and the best-fit background components (epithermal neutron, M-, L_1-, L_2-shell EC) in the alternative hypothesis H_1 when using an exponential approximation for the CEνNS signal (see text). A solid (dotted) line shows the calculated CEνNS signal prediction for MHVE-Fef (MHVE-Lindhard) in the SM.

- Point contact Ge detector
- Dresden II reactor

Colaresi *et al* claims ~ 3σ evidence

(with “optimistic” quenching factor)

CONUS+ experiment

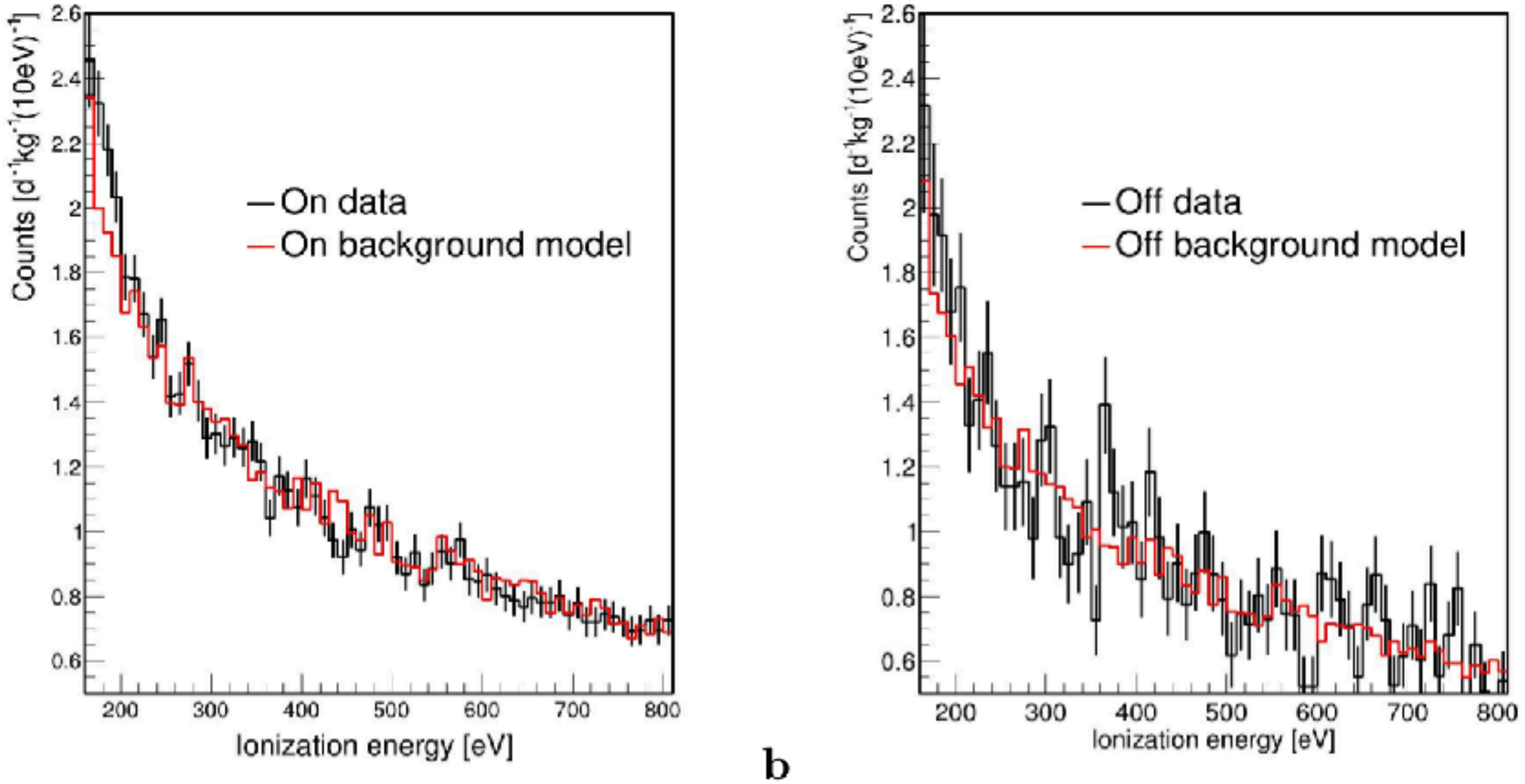

a **b**

Fig. 7: **Data versus model in region of interest. a)** Reactor on and **b)** off count rates normalized to 1 kg day in comparison to the corresponding background models are shown in the region of interest. The signal excess in the reactor on data is seen at low energies below 250 eV_{ee}. The vertical bars represent the statistical uncertainties of the data in each 10 eV_{ee} bin at a 68% CL (1σ). Statistical fluctuations are significantly higher in the off than in the on data due to the shorter period of data collection. Due to the slightly different detector thresholds only one detector (C3) contributes to the lowest bin, the second includes two detectors (C3 and C5) and bins above 180 eV_{ee} are based on the summed spectra of of all three detectors. The difference between the two reactor on curves is shown in figure 3.

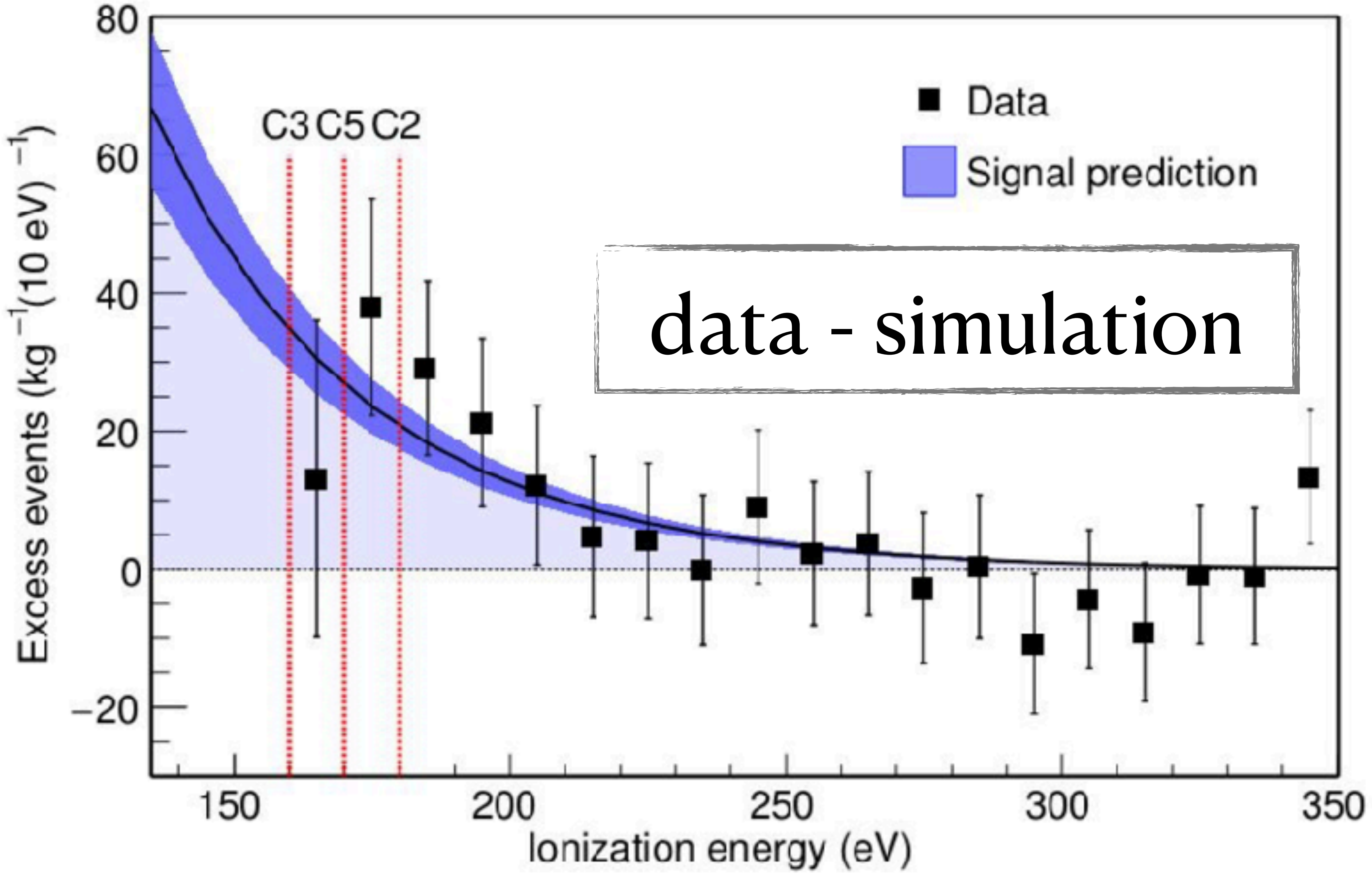

- HPGe detector
- nuclear power plant in Leibstadt, Switzerland

CONUS+ claims 3.7 σ evidence

with quenching in agreement with Lindhart

Outline

- Coherent elastic neutrino nucleus scattering
- The Ricochet experiment
- Commissioning results

Ricochet at the ILL

Ricochet is located at the **research nuclear reactor** (58 MW power) in the Institut Laue-Langevin (ILL) in Grenoble (France)

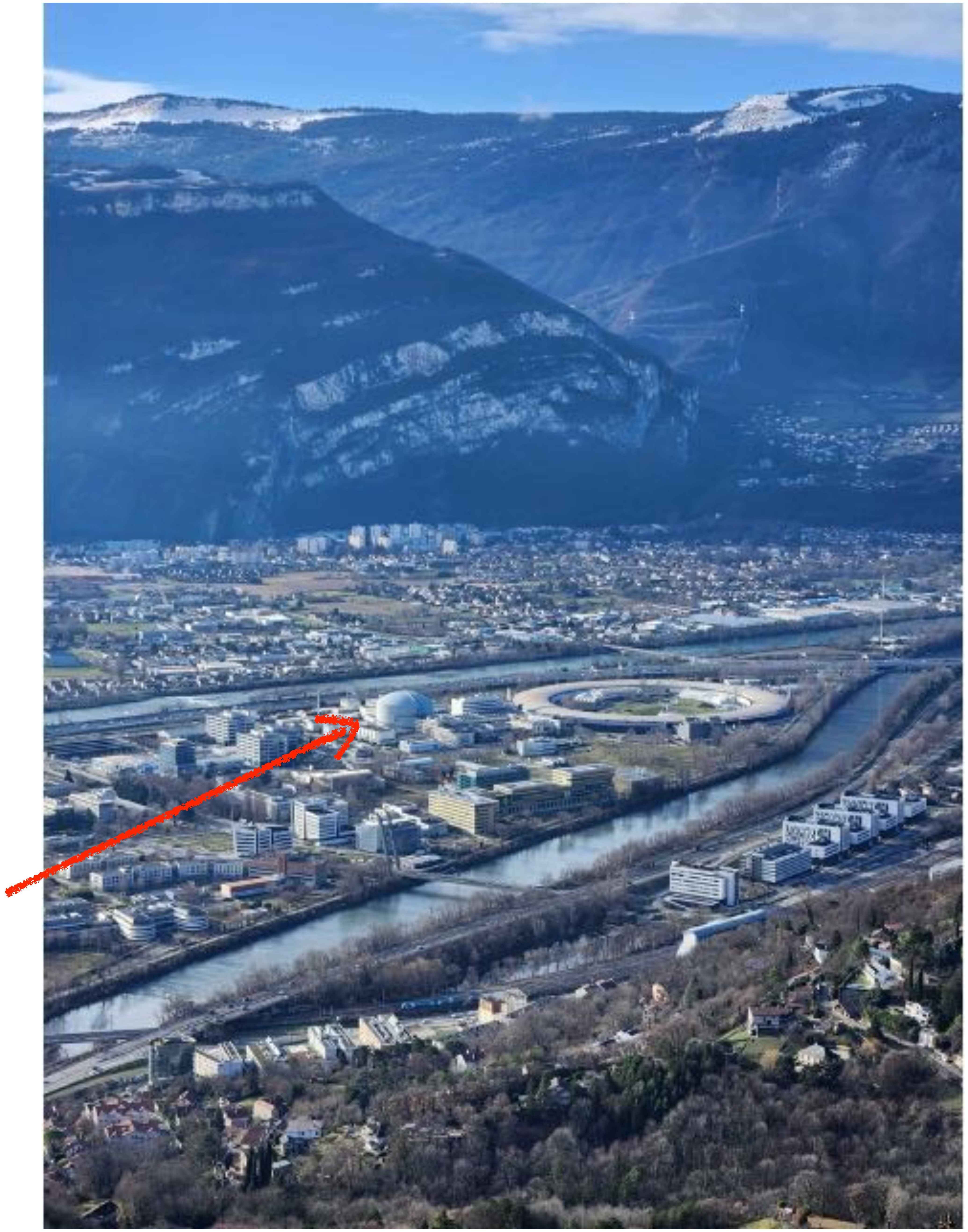

Cryogenic calorimeters

Cryogenic calorimeters are phonon-mediated detectors

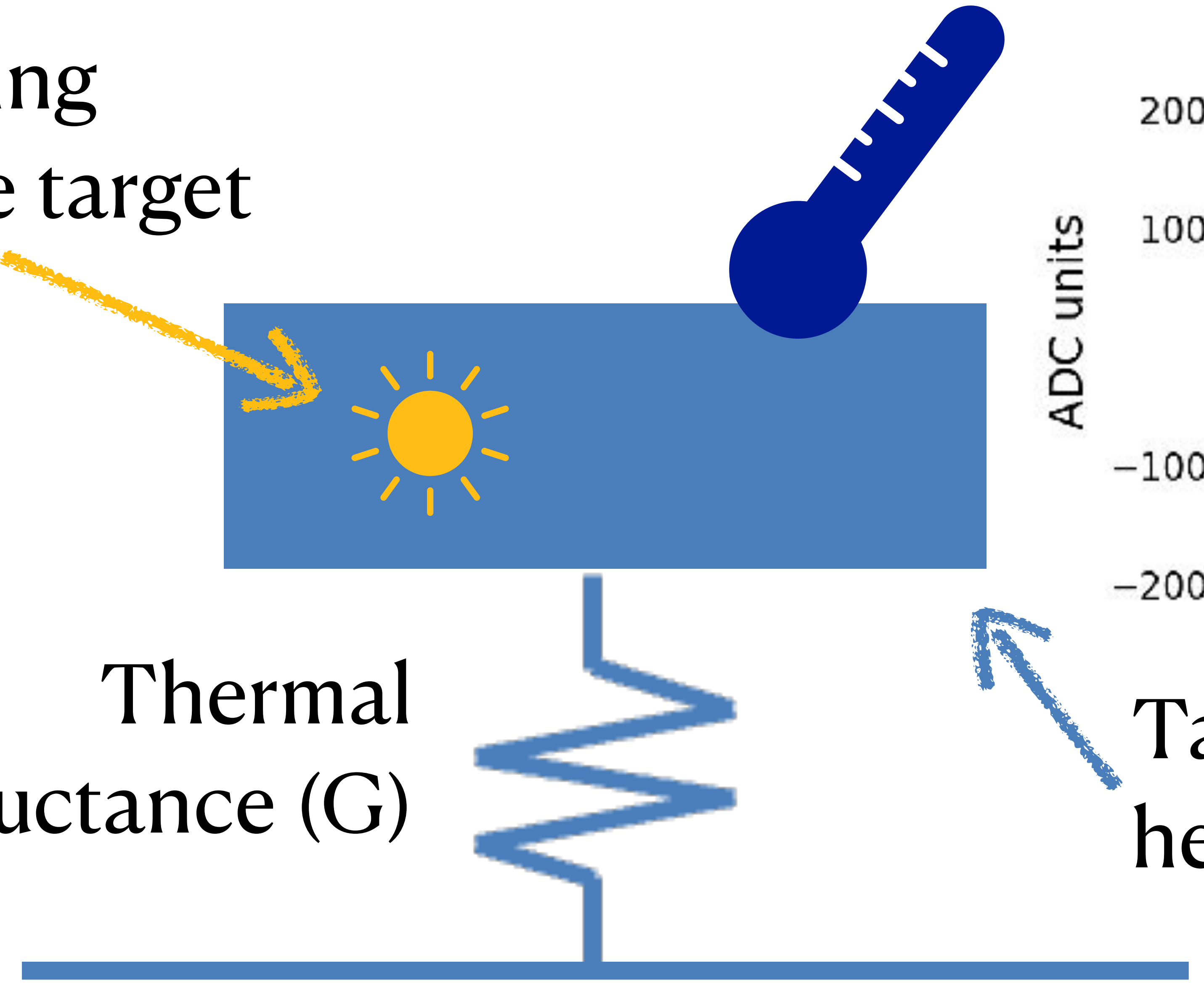

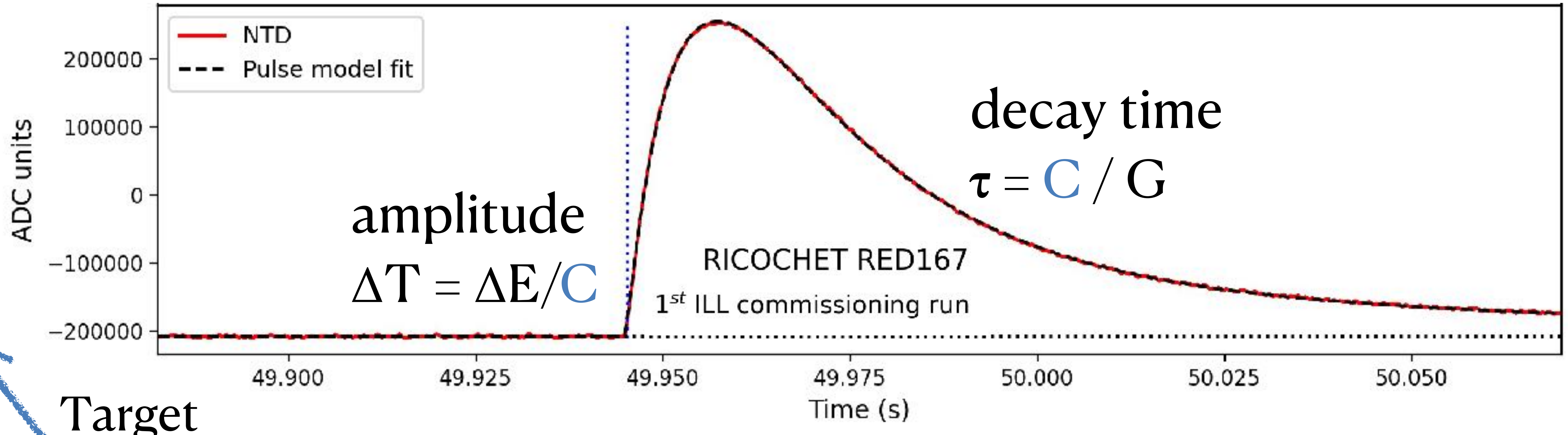

Cryogenic calorimeters have exquisite resolutions and low energy thresholds

C. Augier *et al.*, NIM A, 1057, 168765, (2023) - ArXiv:2304.14926
C. Augier *et al.*, EPJC, 84, 186, (2024) - ArXiv:2306.00166

Two detector technologies

CryoCube

- Neutron-transmutation-doped germanium thermistors for the phonon readout
- Phonon and ionization readout for particle identification
- Germanium targets

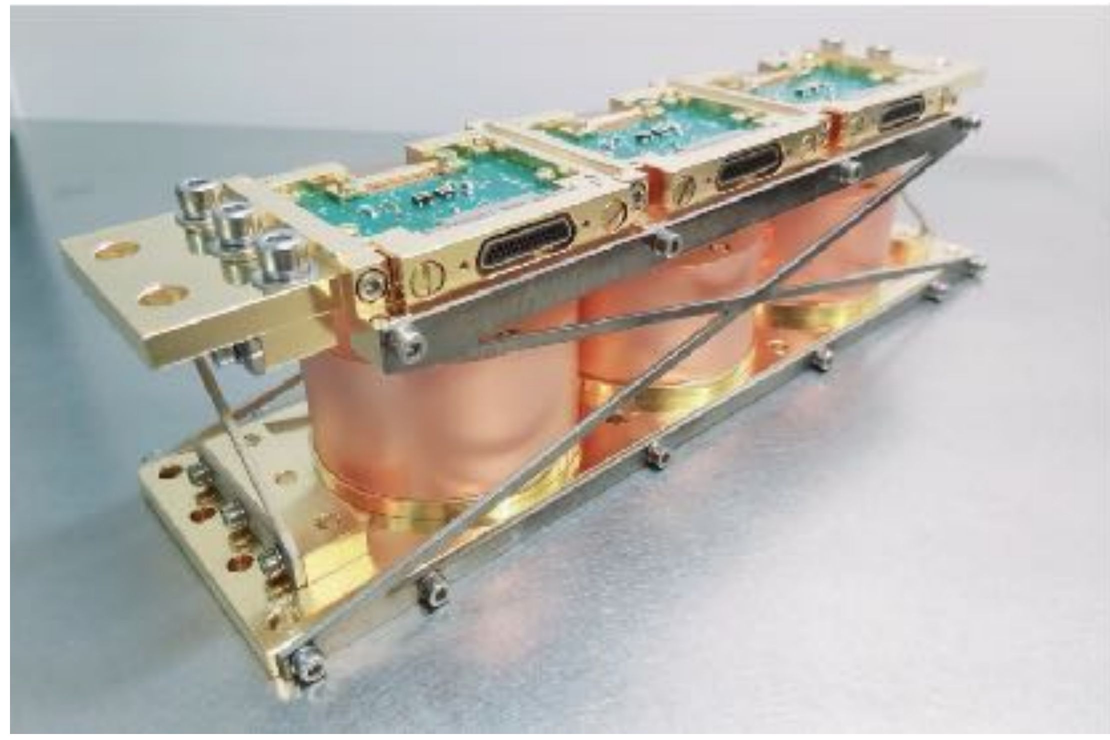

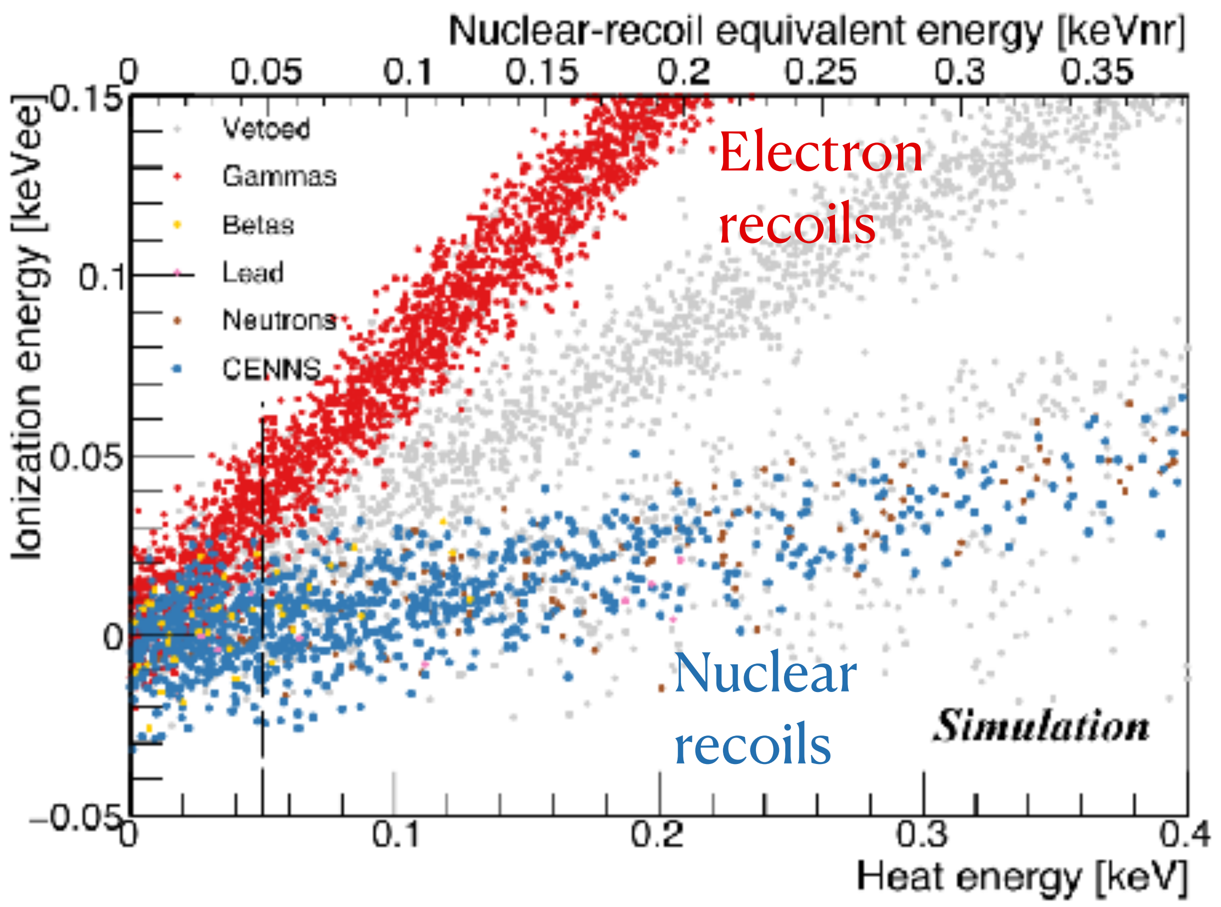

Q-Array

- Transition-Edge Sensor for the phonon readout
- Pulse shape discrimination for particle identification
- Superconducting targets (Zn, Al, Sn)

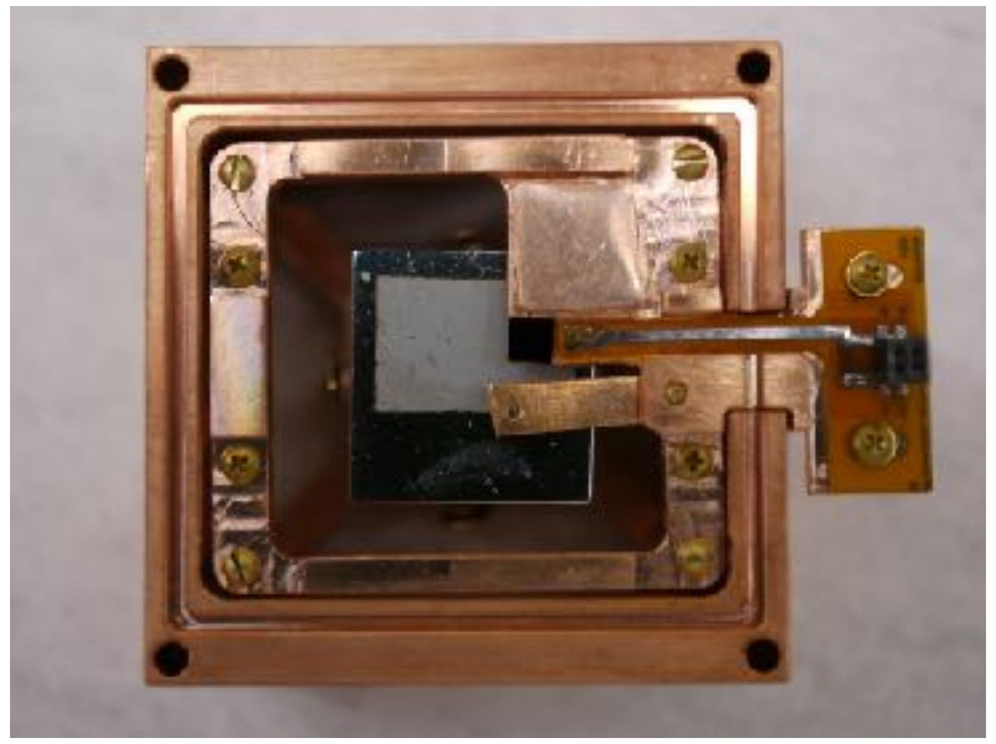

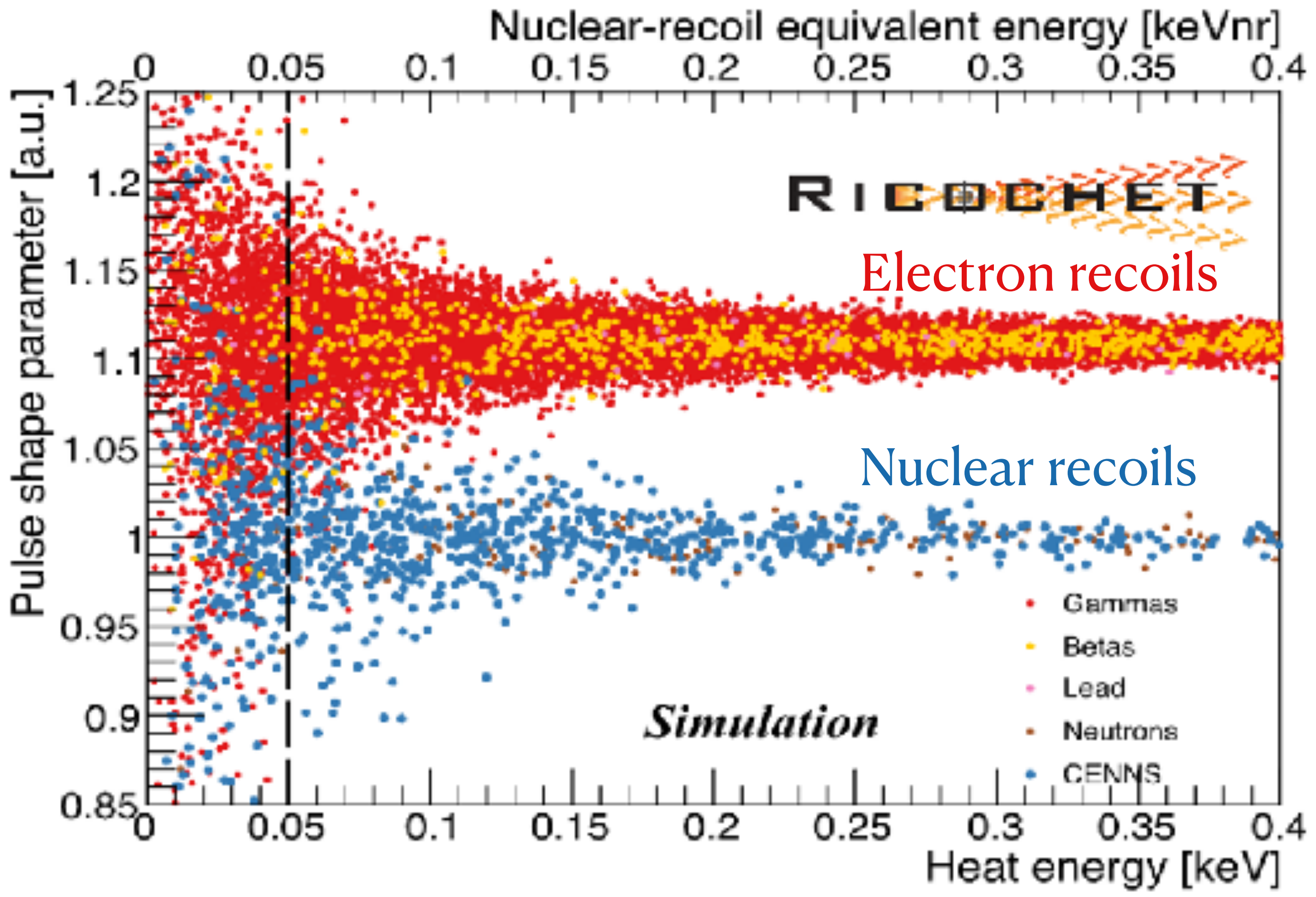

C. Augier *et al.*, NIM A, 1057, 168765, (2023) - ArXiv:2304.14926
C. Augier *et al.*, EPJC, 84, 186, (2024) - ArXiv:2306.00166

Two detector technologies

CryoCube

- Neutron-transmutation-doped germanium thermistors for the phonon readout
- Phonon and ionization readout for particle identification
- Germanium targets

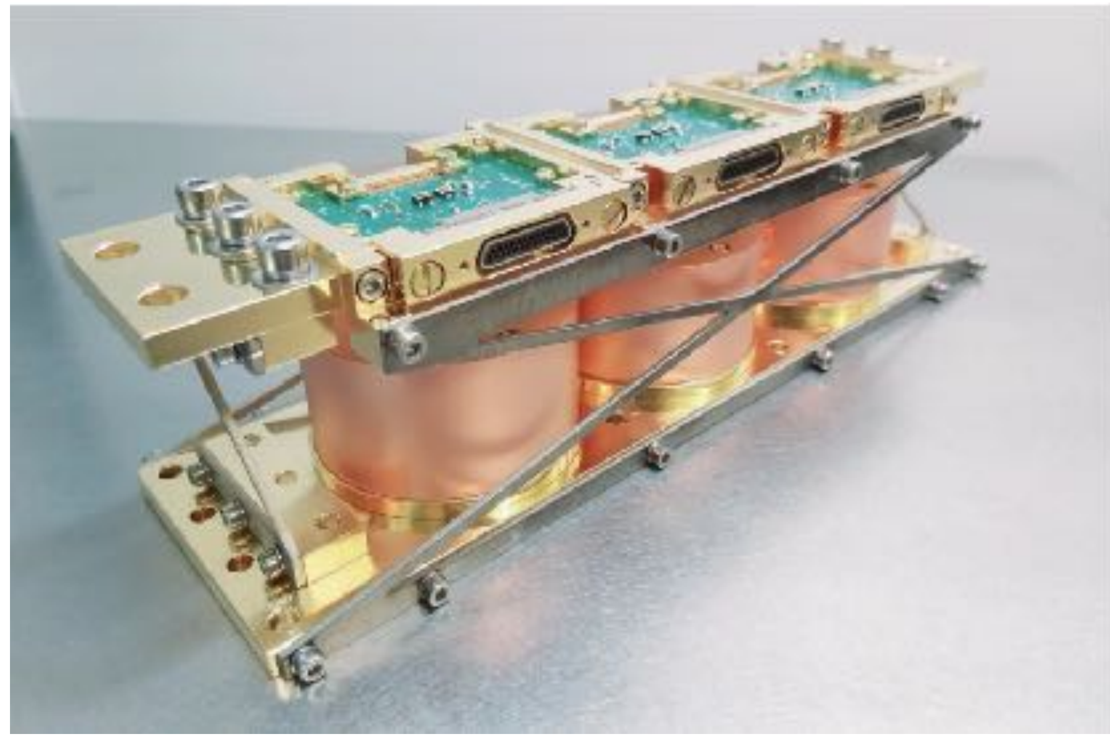

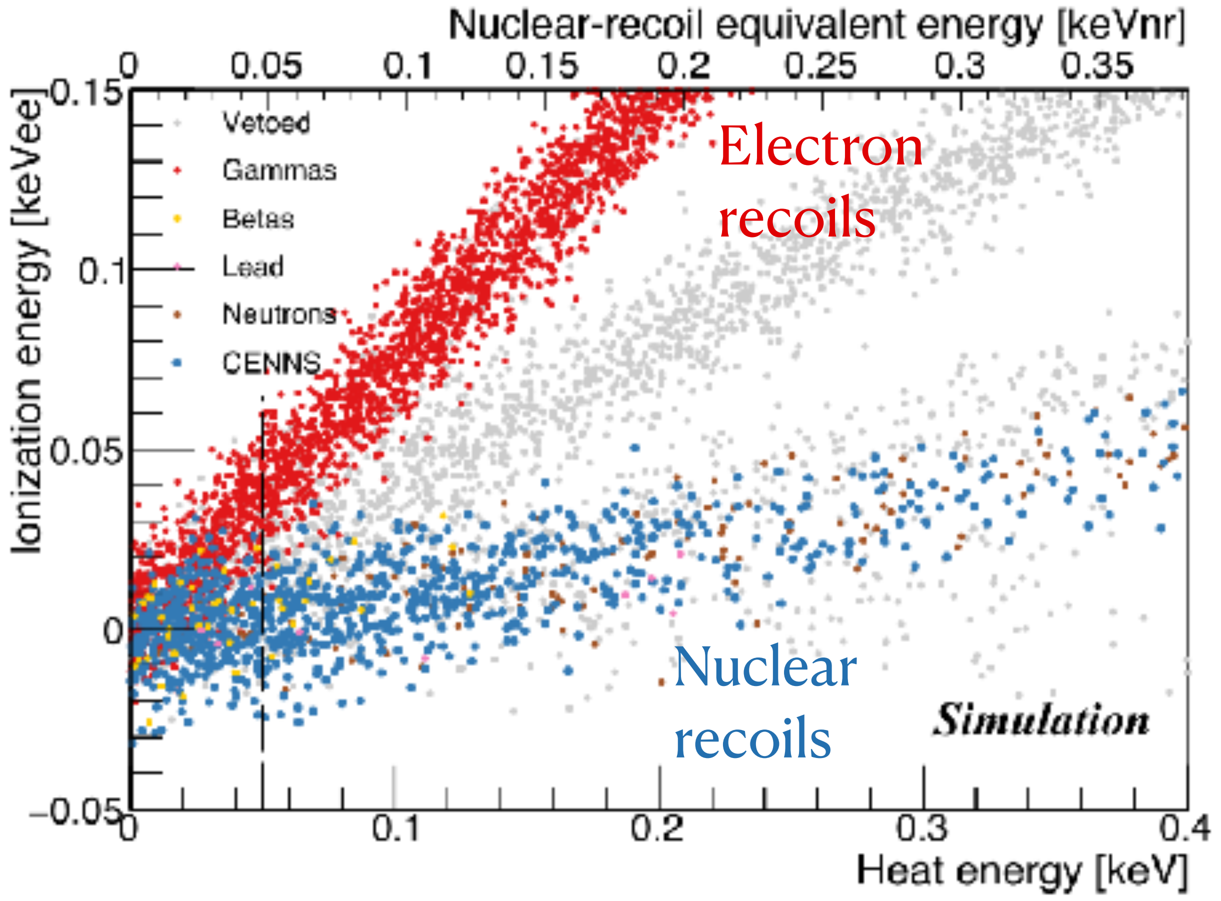

Q-Array

- Transition-Edge Sensor for the phonon readout
- Pulse shape discrimination for particle identification
- Superconducting targets (Zn, Al, Sn)

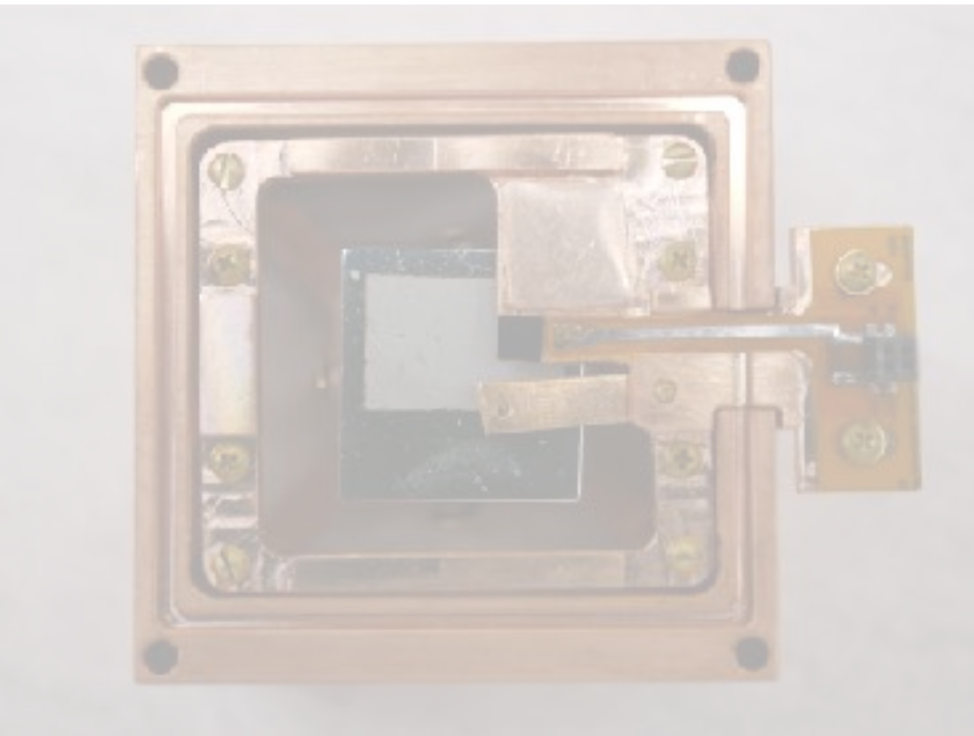

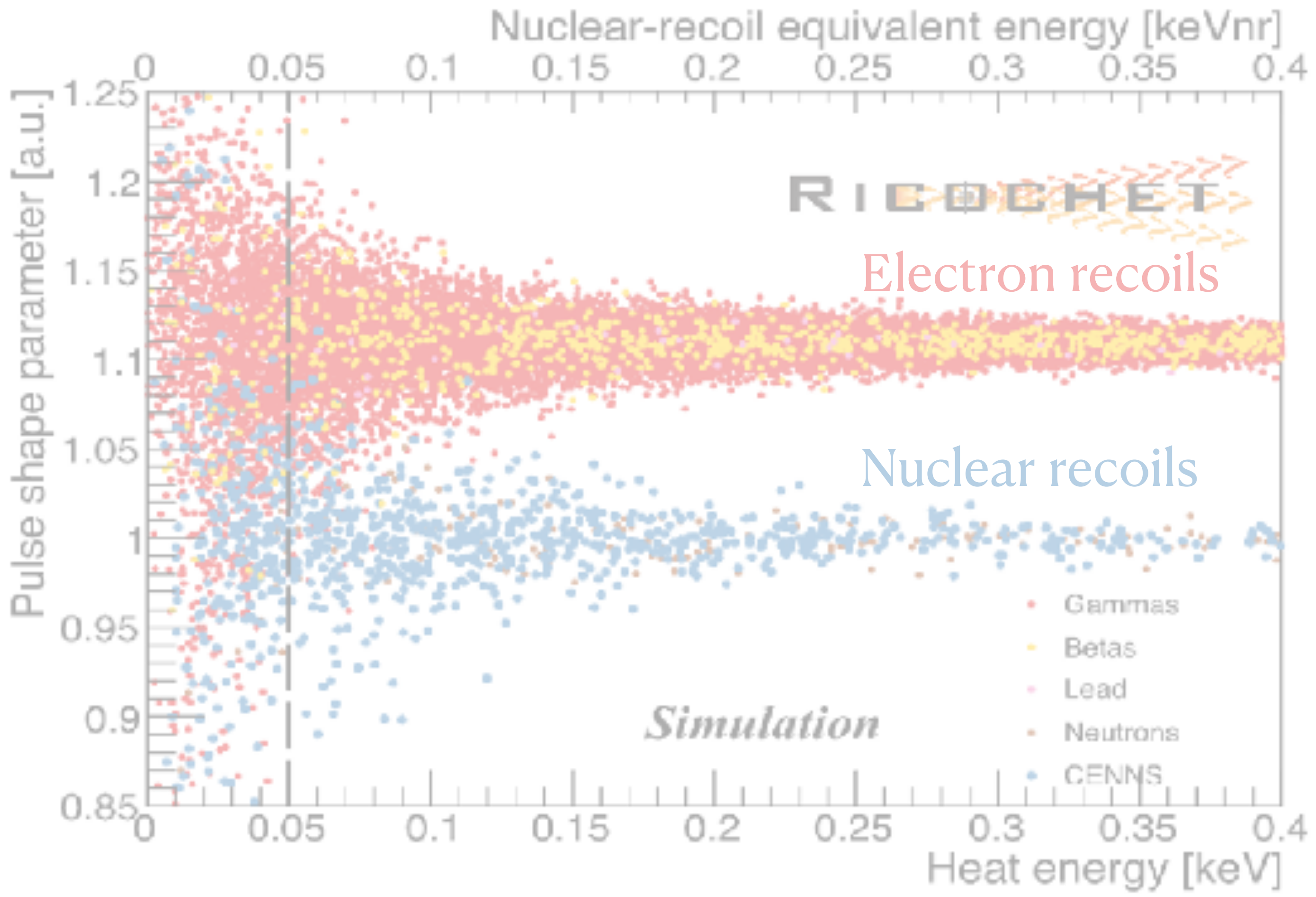

Neganov-Trofimov-Luke effect

$$E_{ph} = E_r + E_{NTL} = E_r \left(1 + Q\frac{e \cdot V}{\epsilon}\right)$$

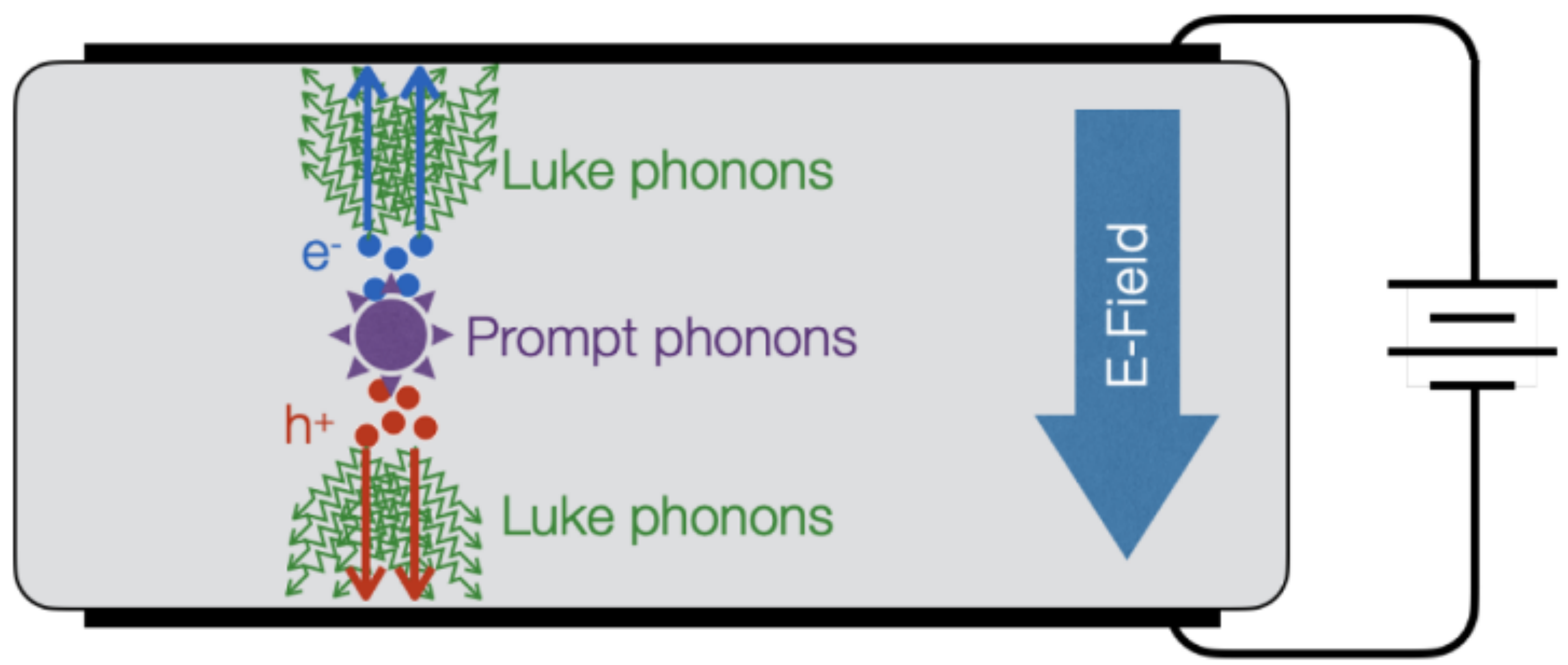

- Total phonon energy (keV_{ph})

$$E_{ph} = E_r + E_{NTL} = E_r \left(1 + Q\frac{q \cdot V}{\epsilon}\right)$$

- Ionization energy (keV_{ee})

$$E_{ion}$$

- Recoil energy (keV)

$$E_r = E_{ph} - E_{ion}\left(q\frac{V}{\epsilon}\right)$$

B. S. Neganov and V. N. Trofimov, Otkryt. Izobret., 146, 215 (1985)
P. N. Luke, J. Applied Phys. 64,6858 (1988)

CryoCube: two electrode geometries

Planar electrode geometry

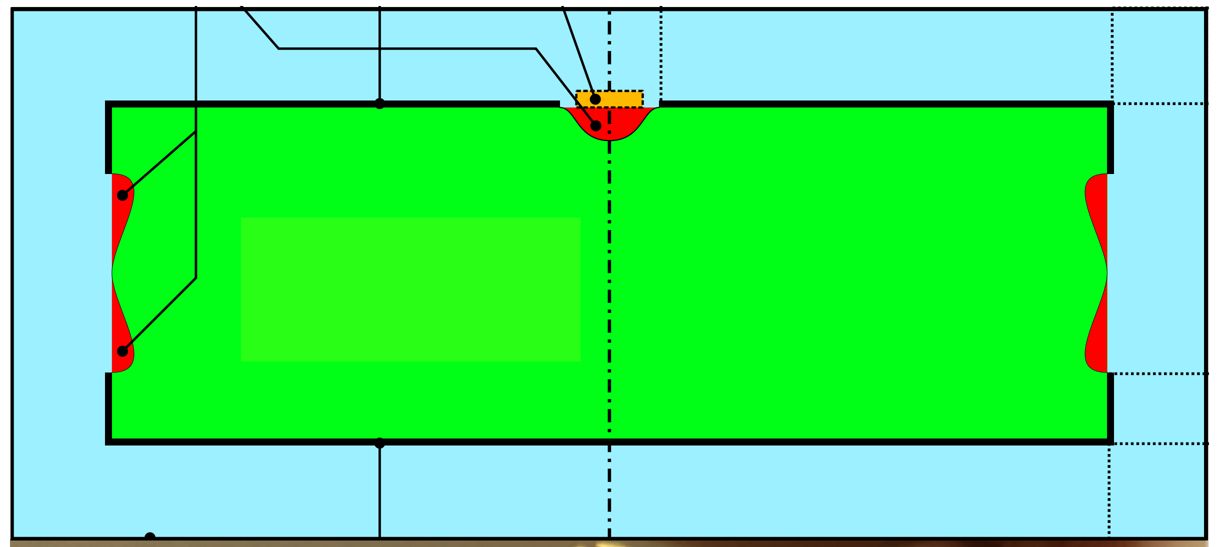

Fully Inter-Digitized (FID) electrode geometry

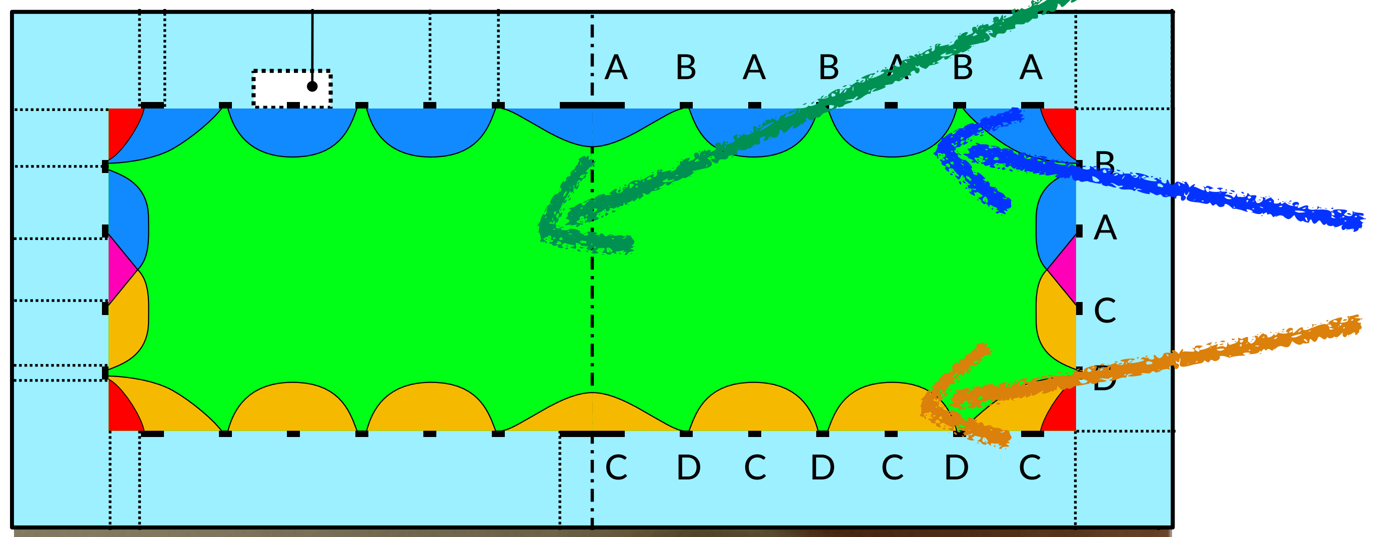

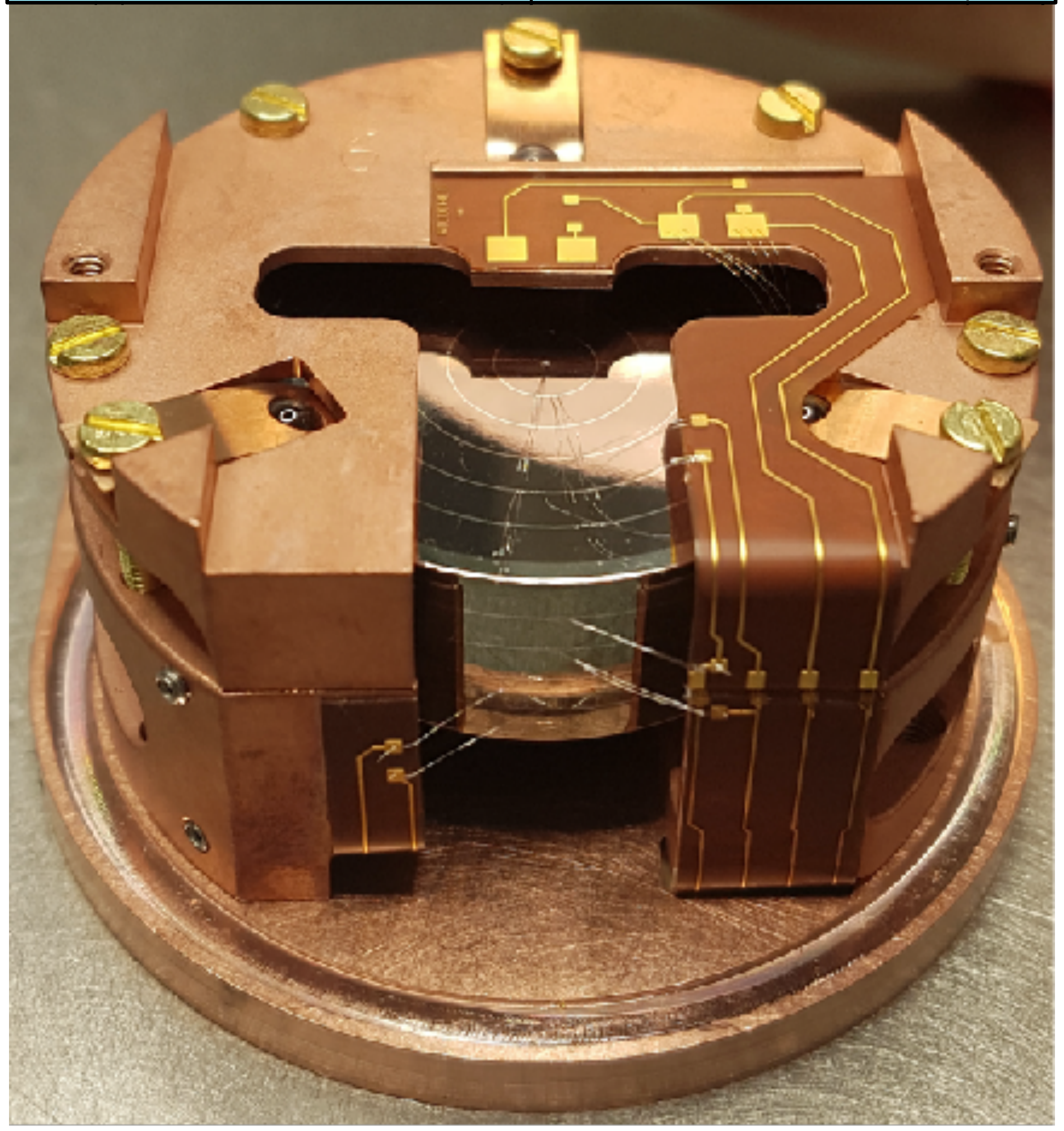

Planar geometry:

- No surface event discrimination
- All the volume is sensitive

FID geometry:

- Surface event discrimination
- Reduced sensitive volume

Background mitigation

Cosmogenic, reactogenic and radiogenic background rejection:

- 15 m water equivalent overburden from the water transfer channel

Background mitigation

Cosmogenic, reactogenic and radiogenic background rejection:

- 15 m water equivalent overburden from the water transfer channel
- Active outer muon veto

Background mitigation

Cosmogenic, reactogenic and radiogenic background rejection:

- 15 m water equivalent overburden from the water transfer channel
- Active outer muon veto
- Outer shielding (Pb, HDPE, soft iron)

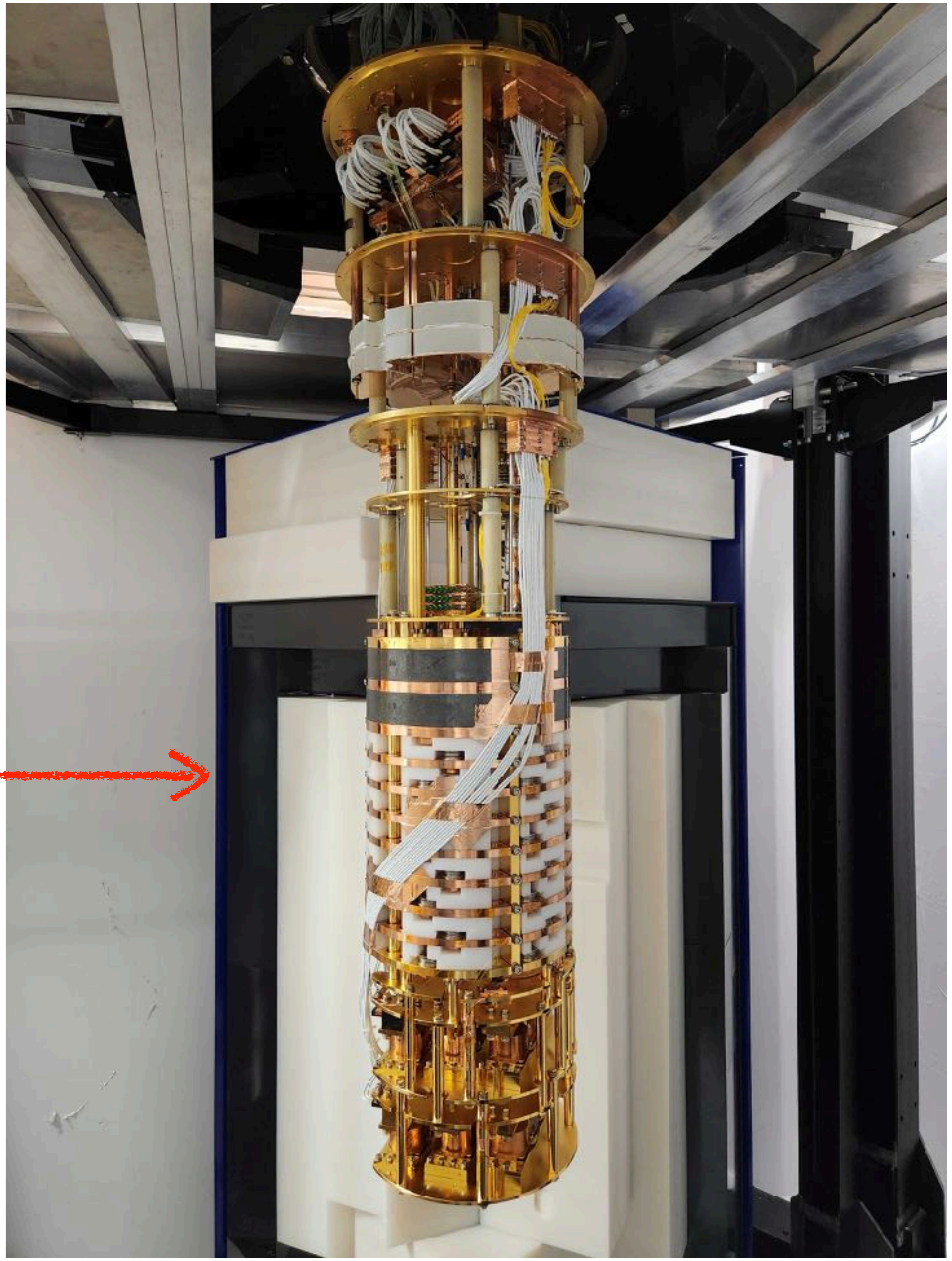

Background mitigation

Cosmogenic, reactogenic and radiogenic background rejection:

- 15 m water equivalent overburden from the water transfer channel
- Active outer muon veto
- Outer shielding (Pb, HDPE, soft iron)
- Additional inner shielding HDPE sheets at 1K, 4K and 50K

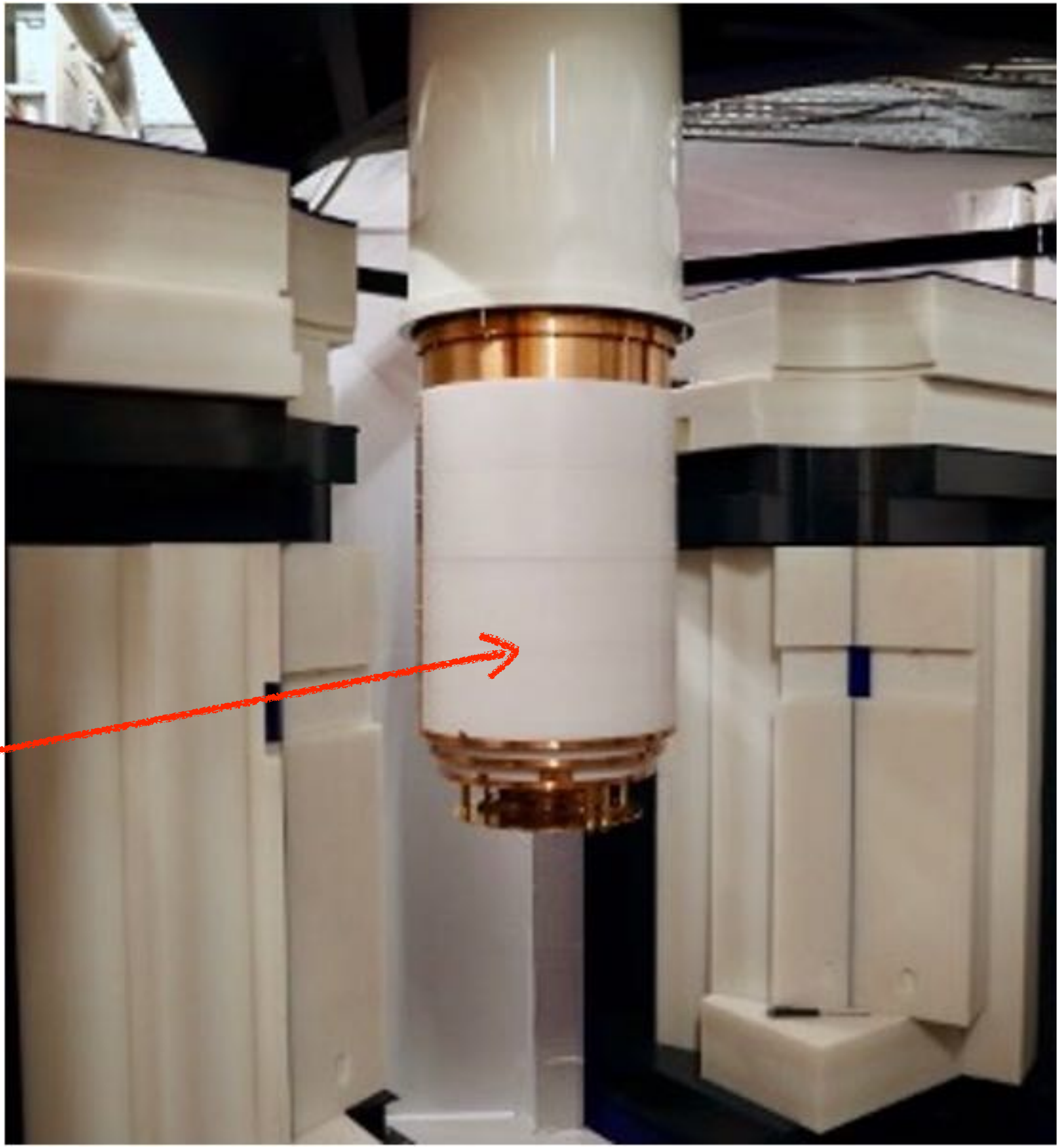

Background mitigation

Cosmogenic, reactogenic and radiogenic background rejection:

- 15 m water equivalent overburden from the water transfer channel
- Active outer muon veto
- Outer shielding (Pb, HDPE, soft iron)
- Additional inner shielding HDPE sheets at 1K, 4K and 50K
- Cryogenic muon veto

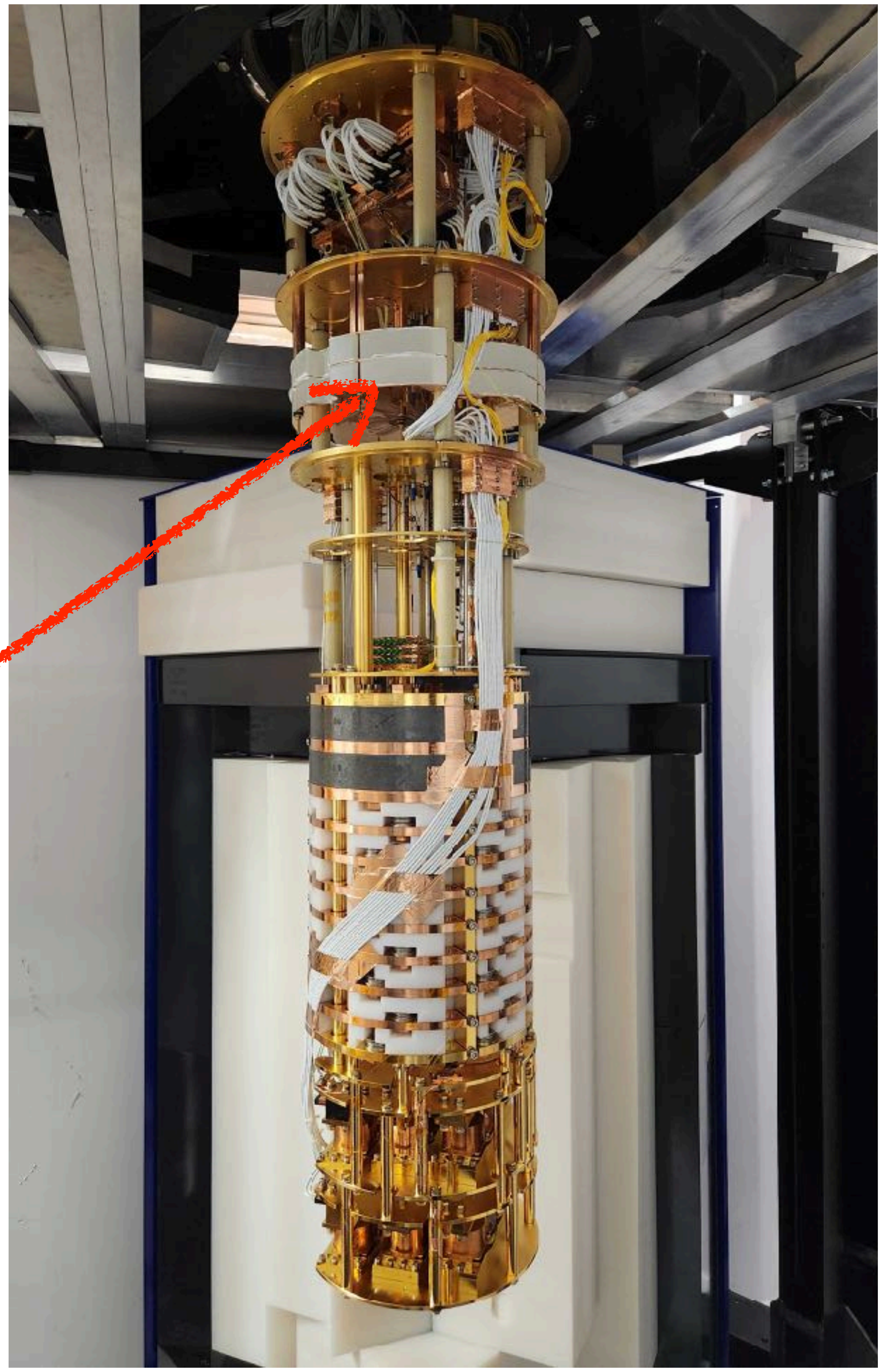

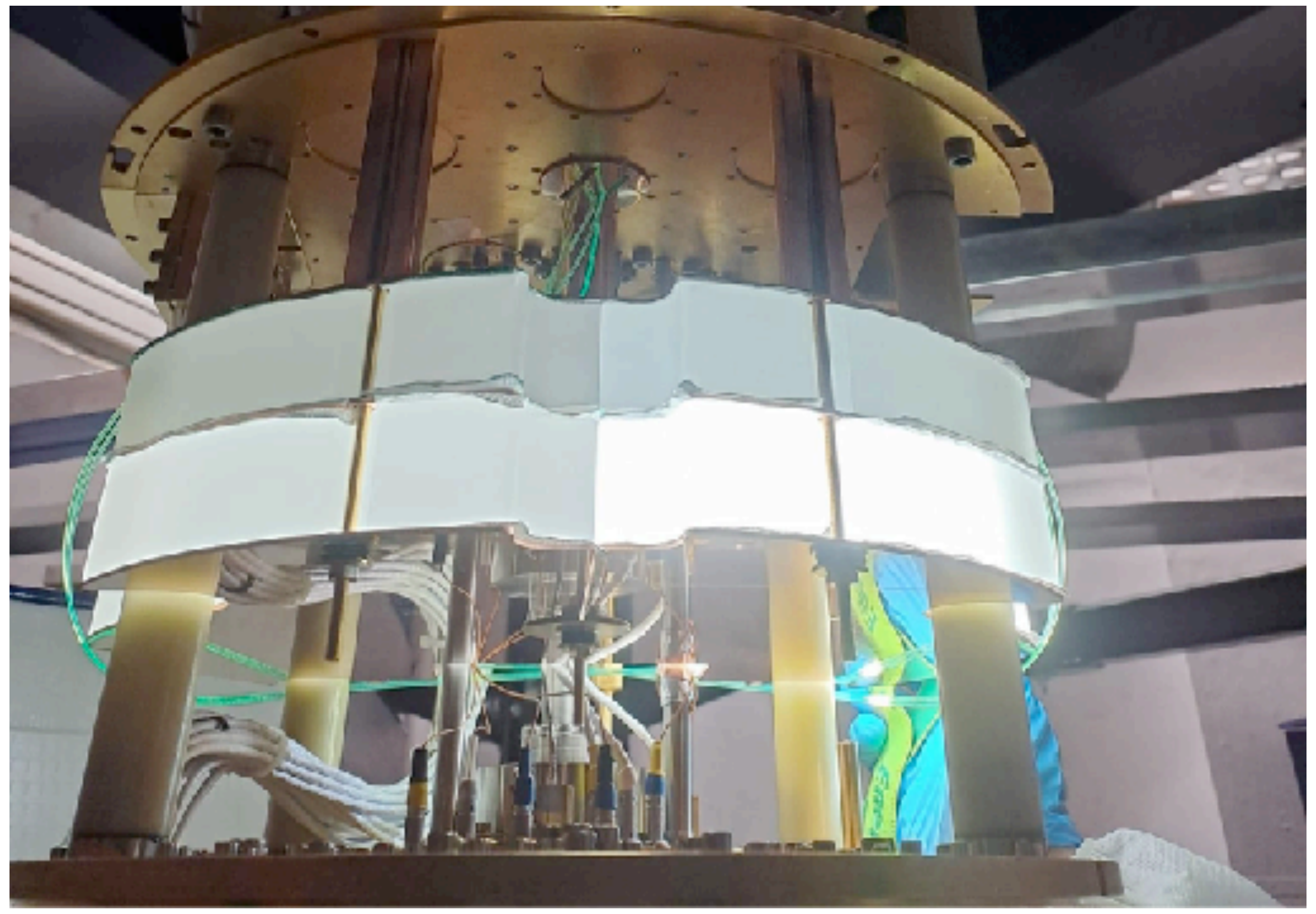

Background mitigation

Cosmogenic, reactogenic and radiogenic background rejection:

- 15 m water equivalent overburden from the water transfer channel
- Active outer muon veto
- Outer shielding (Pb, HDPE, soft iron)
- Additional inner shielding HDPE sheets at 1K, 4K and 50K
- Cryogenic muon veto
- Inner shielding at 1K (Pb, Cu and HDPE)

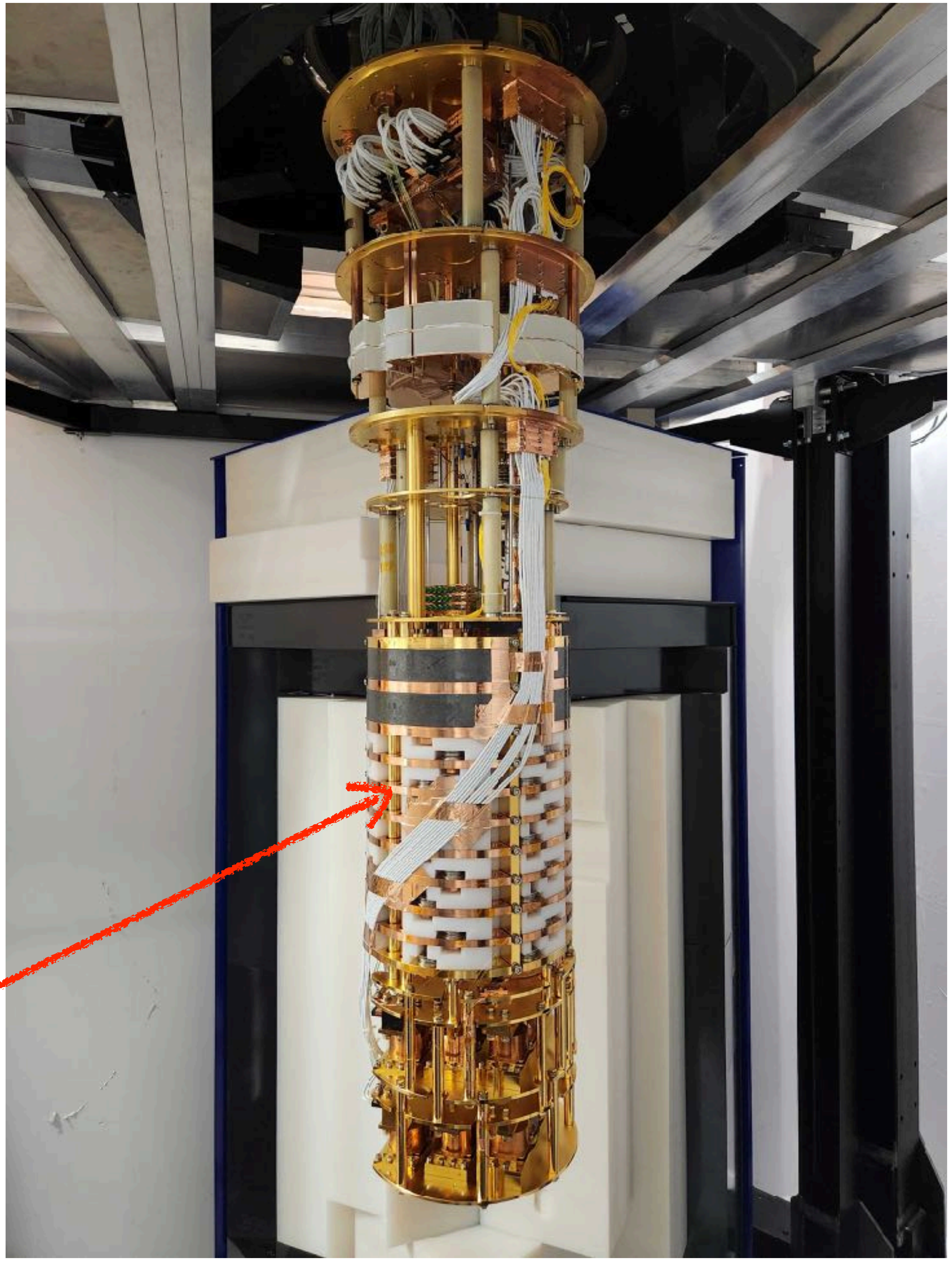

Outline

- Coherent elastic neutrino nucleus scattering
- The Ricochet experiment
- Commissioning results

Installation at the ILL

Nov. 8th, 2023

Nov. 20th, 2023

Dec. 5th, 2023

Jan. 9th, 2024

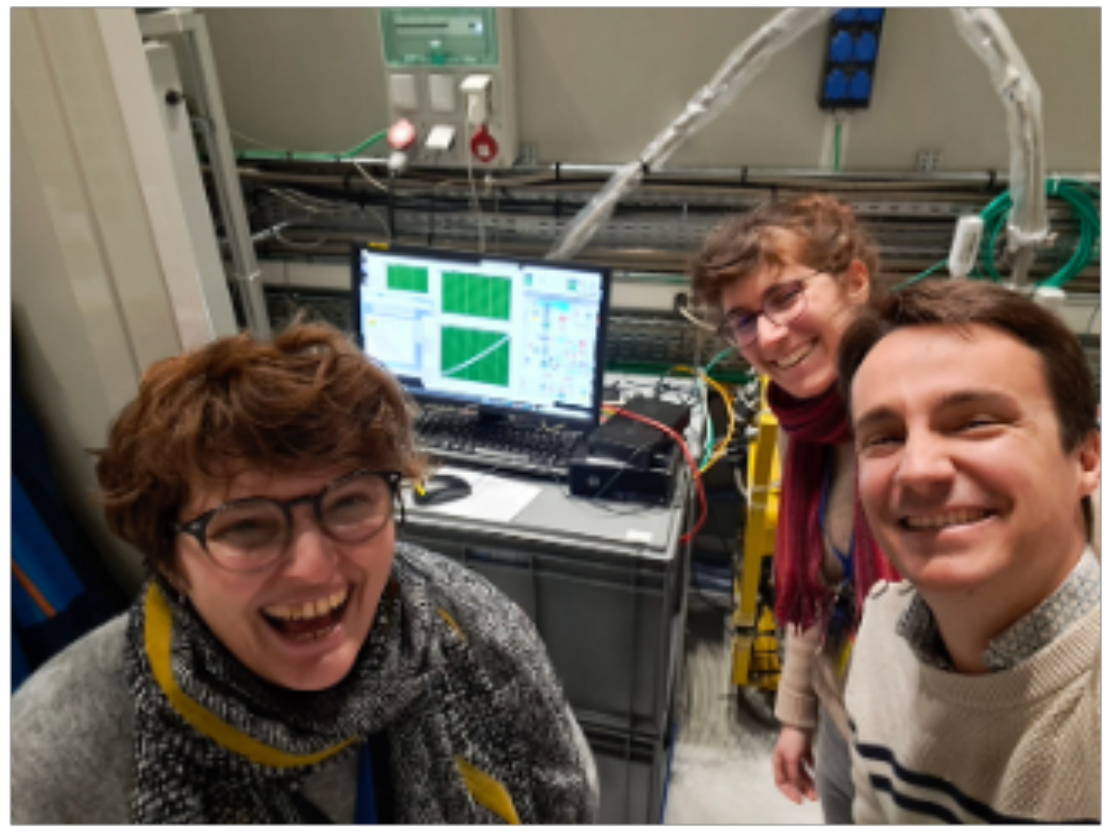

Feb. 6th, 2024

Commissioning at the ILL

Four commissioning cryogenic runs from February 2024 to June 2025 to test the various sub-systems in a controlled way

Commissioning

Cryogenic commissioning:

- empty cryostat with part of the cabling and thermometry
- a base temperature of 8.8 mK was achieved

RUN012

→

Feb. 2024 | Apr. 2024 | May 2024 | Oct. 2024 | Jan. 2025 | Jun. 2025 | Jul. 2025

A. Armatol *et al.*, arXiv:2507.22751 (2025)

Commissioning

Detector commissioning:
first measurement of one mini-CryoCube
with planar electrodes at the ILL
(three 42-gram germanium cryogenic calorimeters)

- test of detector performance with reactor on/off
- mitigation of vibrations

⟶ **RUN013**

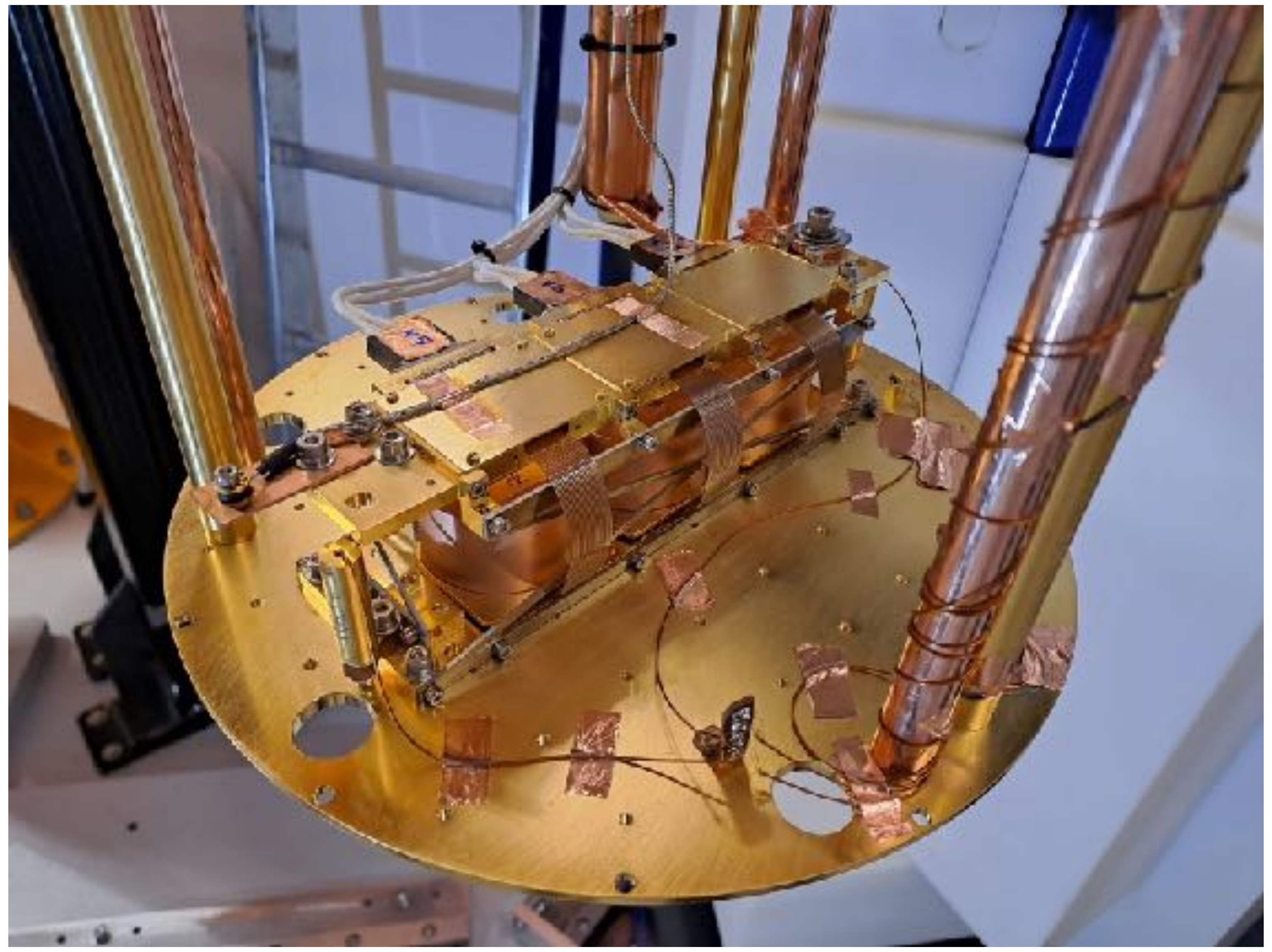

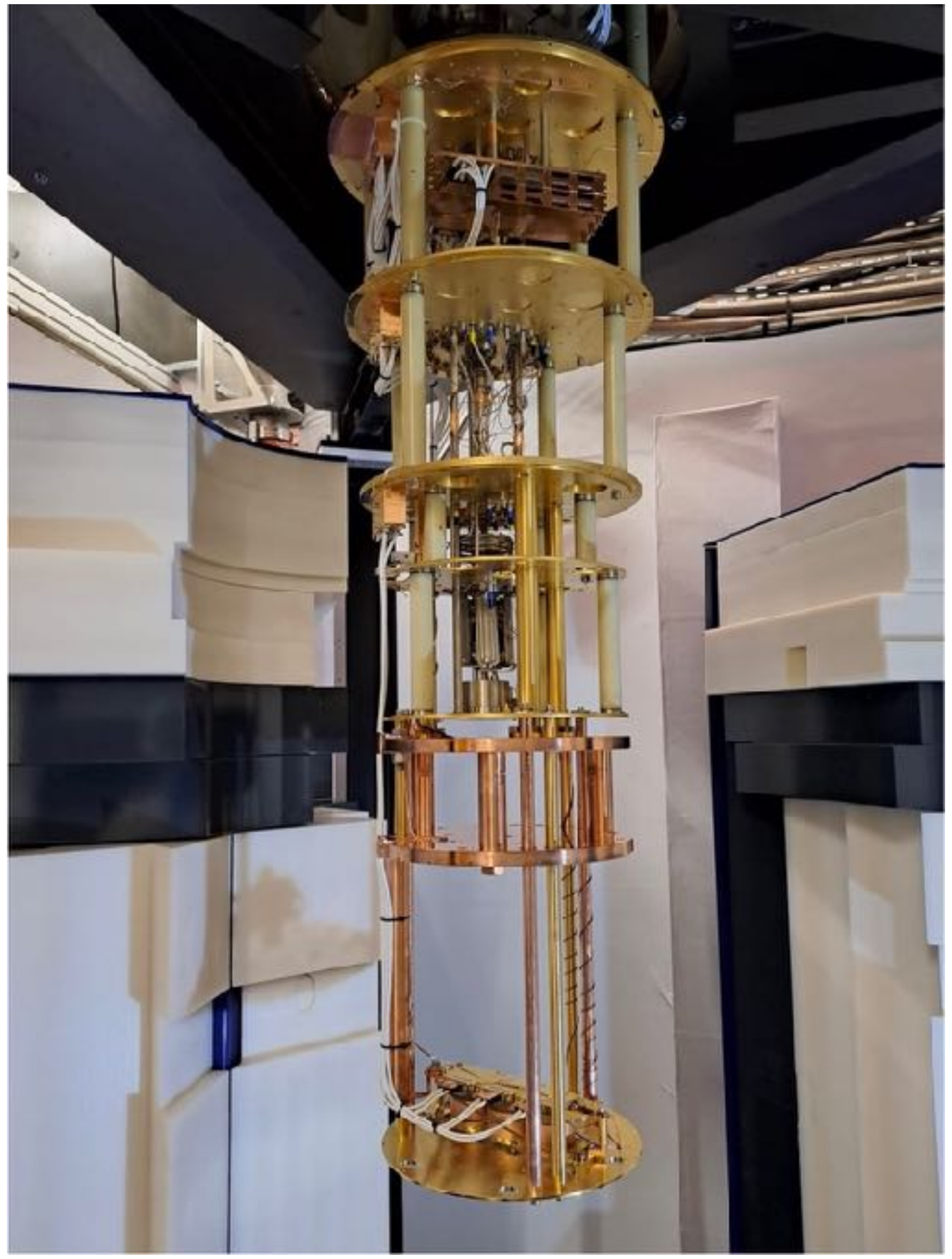

Feb. 2024 | Apr. 2024 | May 2024 | Oct. 2024 | Jan. 2025 | Jun. 2025 | Jul. 2025

Commissioning

Background commissioning:

- Payload of one mini-CryoCube with planar geometry
- Inner shielding
- Laser system
- External muon veto

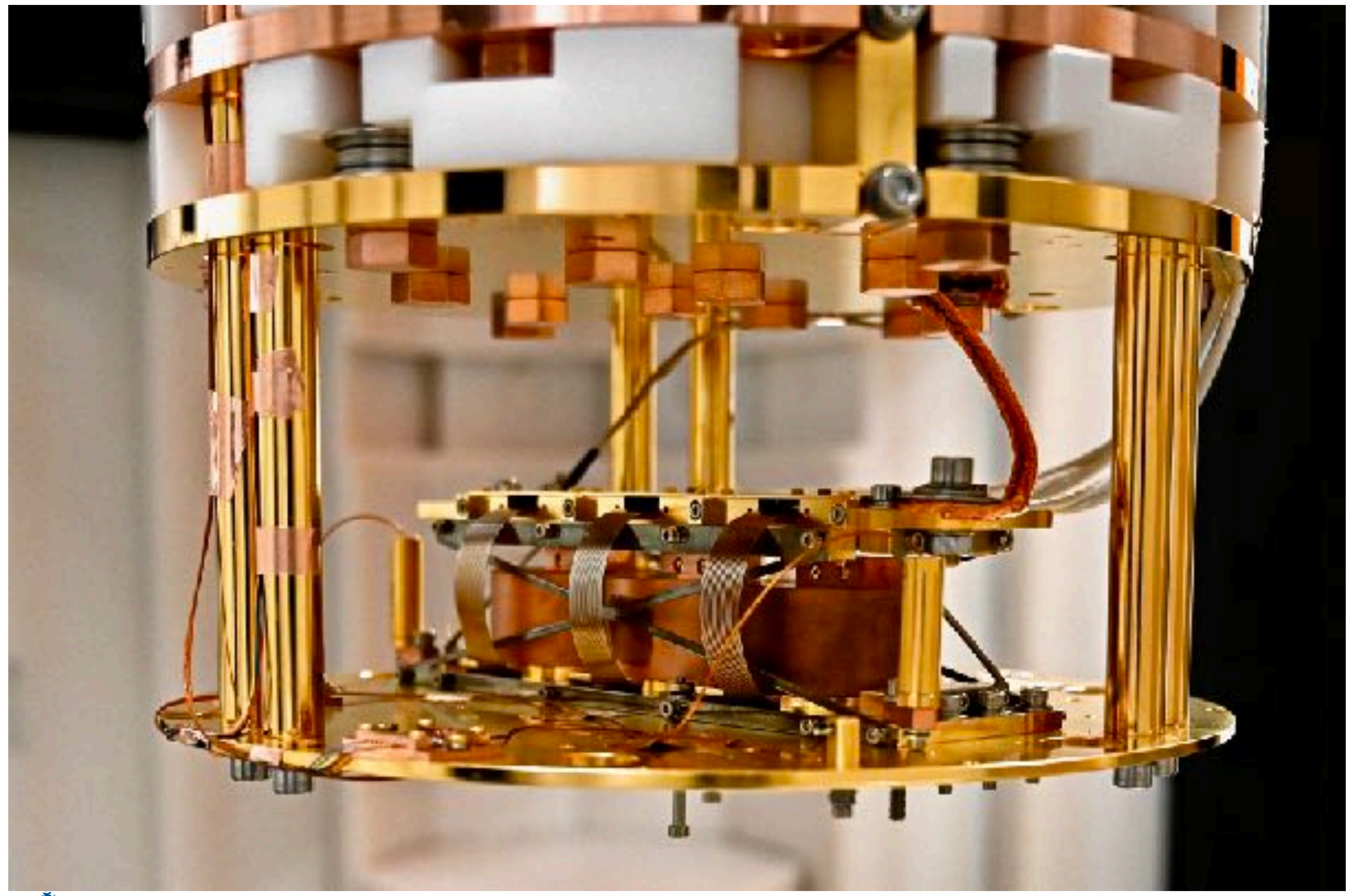

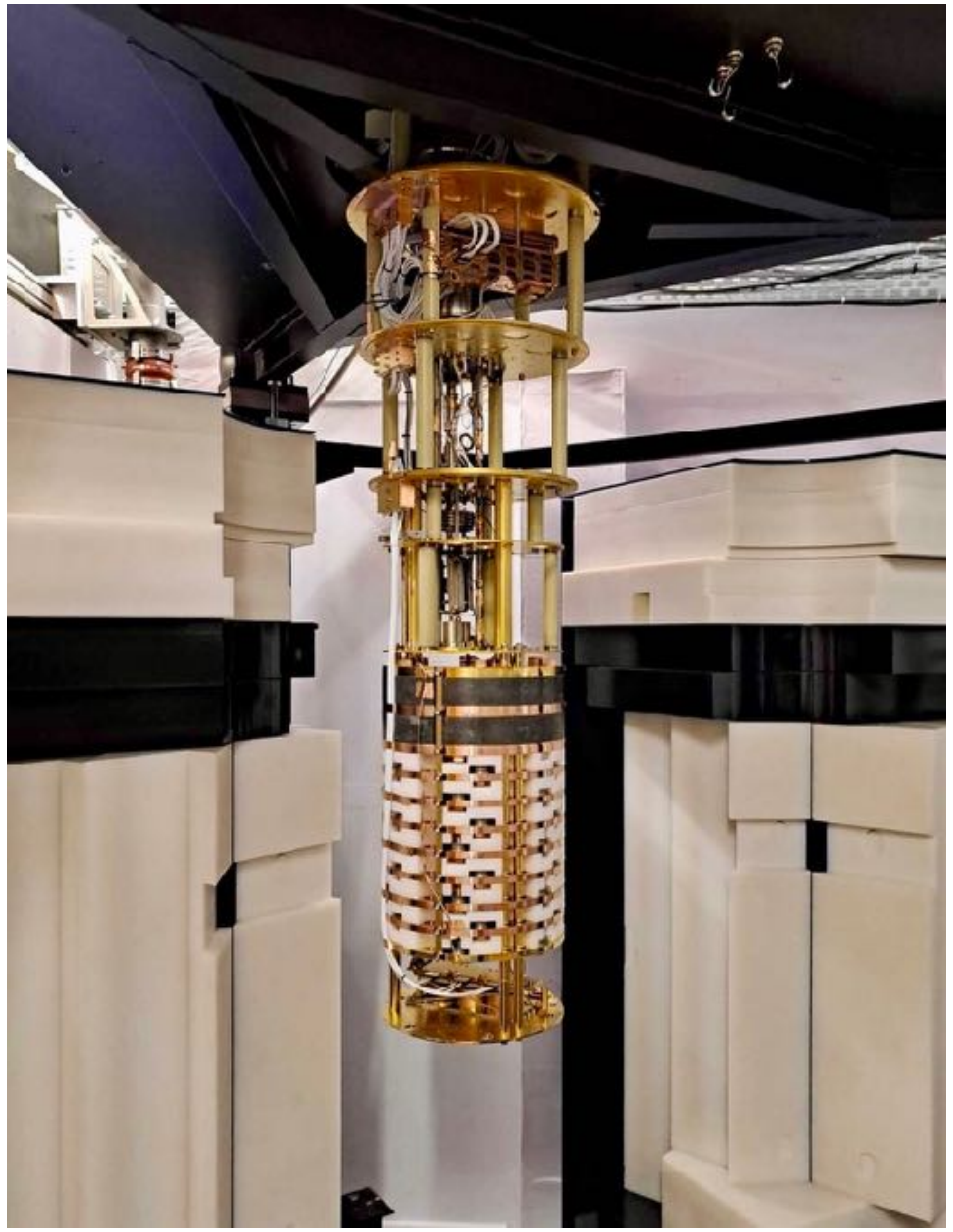

RUN014 →

Feb. 2024 | Apr. 2024 | May 2024 | Oct. 2024 | Jan. 2025 | Jun. 2025 | Jul. 2025

A. Armatol *et al.*, arXiv:2507.22751 (2025)

Data selections

- Low-frequency χ^2 selection on phonon channel
- Pre-pulse mean baseline of the ionization channel

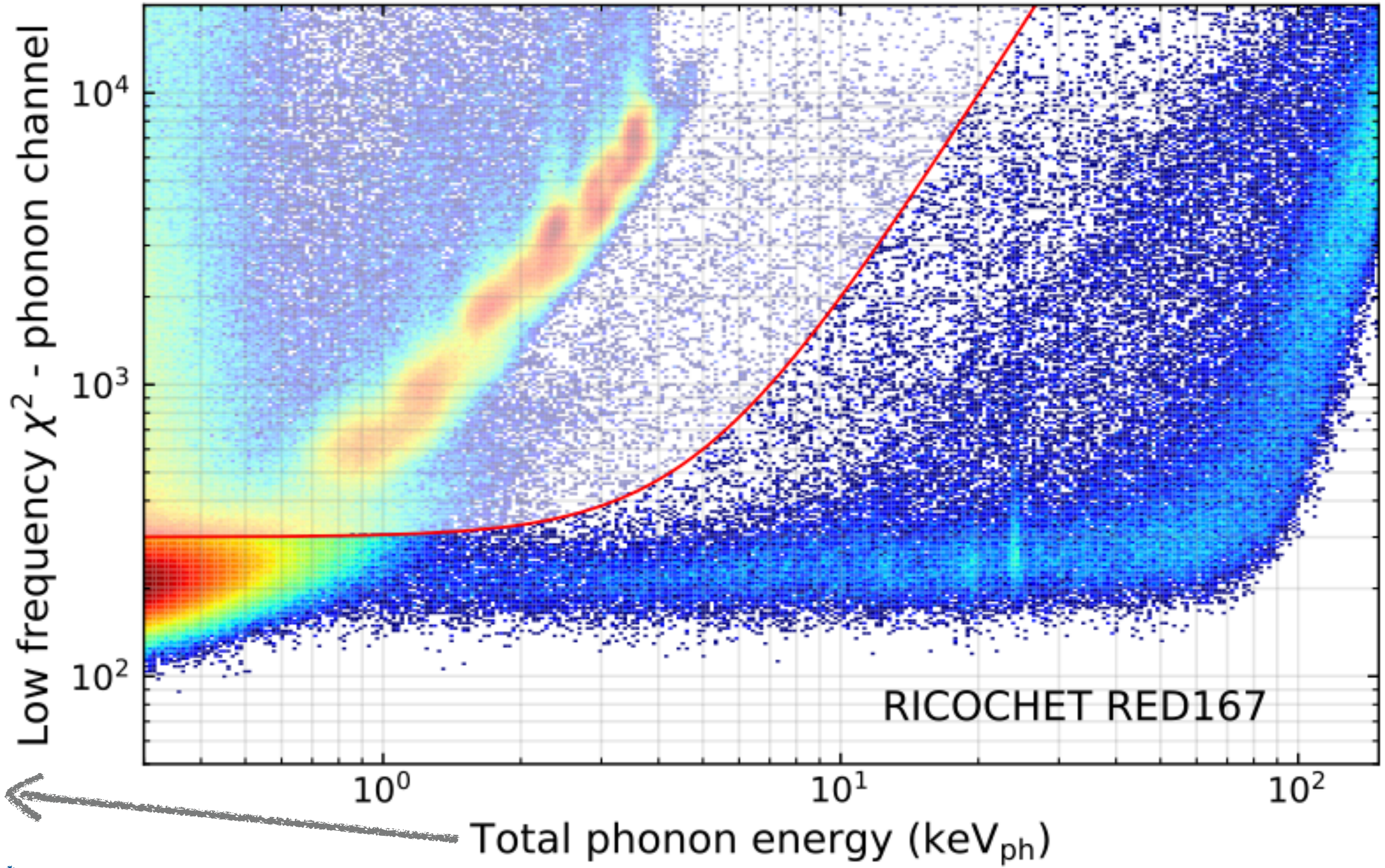

$$E_{ph} = E_r + E_{NTL}$$

RUN014

A. Armatol *et al.*, arXiv:2507.22751 (2025)

Resolution performance

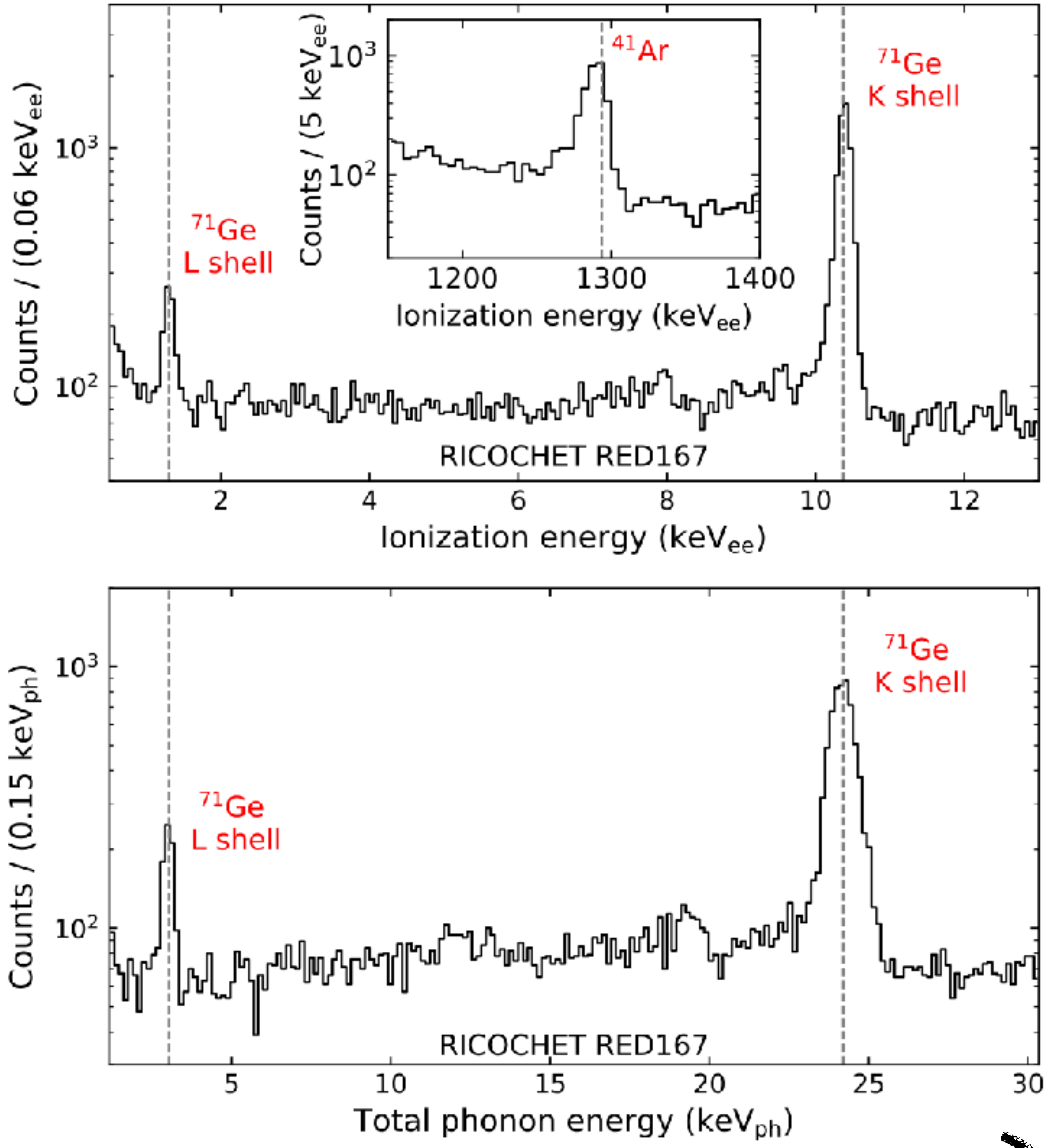

Detector performance improvement during the commissioning phase through vibration mitigation.

At the end of RUN014:

- ionization baseline resolution σ = 40 eV$_{ee}$
- phonon baseline resolution σ = 50 eV$_{ph}$ - 80 eV$_{ph}$

RUN014

Feb. 2024 | Apr. 2024 | May 2024 | Oct. 2024 | Jan. 2025 | Jun. 2025 | Jul. 2025

Trigger and data selection efficiency

- CEvNS signal < 2 keV in Ge
- Commissioning ROI: 2-7 keV
  - Avoid CEvNS
  - Avoid L shell (1.3 keV) and K shell (10.37 keV) of ^{71}Ge
  - Avoid Cu x-ray fluorescence at 8.1 keV

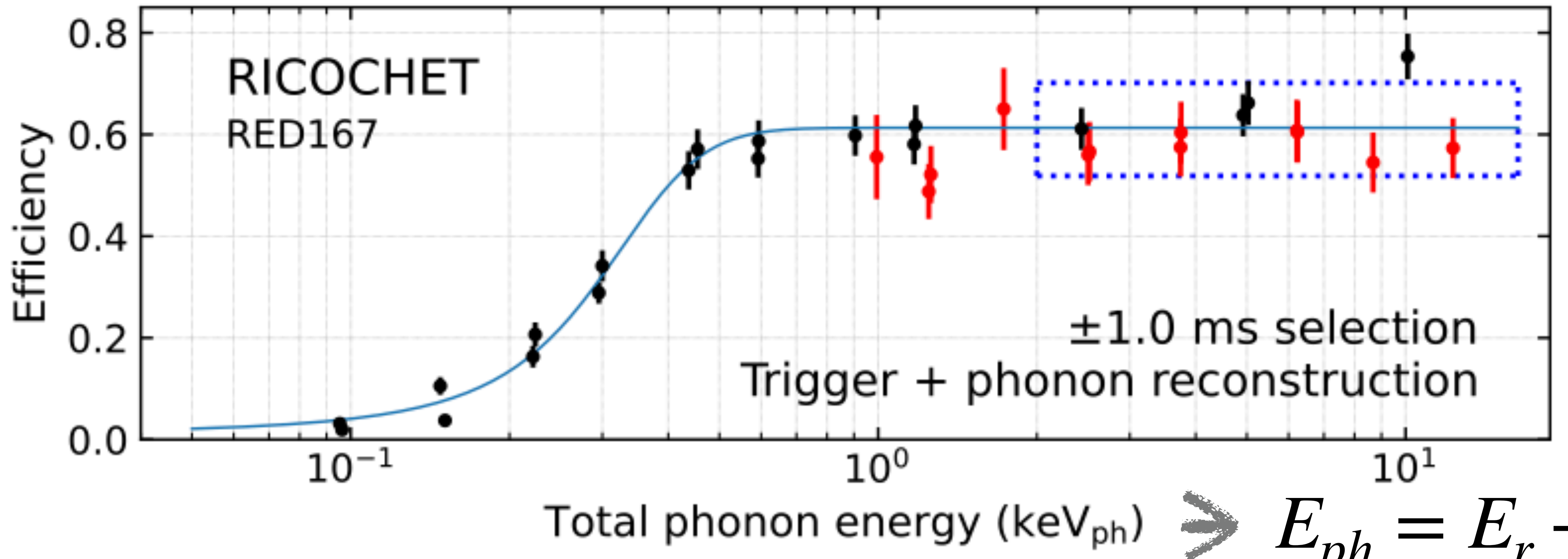

→ $E_{ph} = E_r + E_{NTL}$

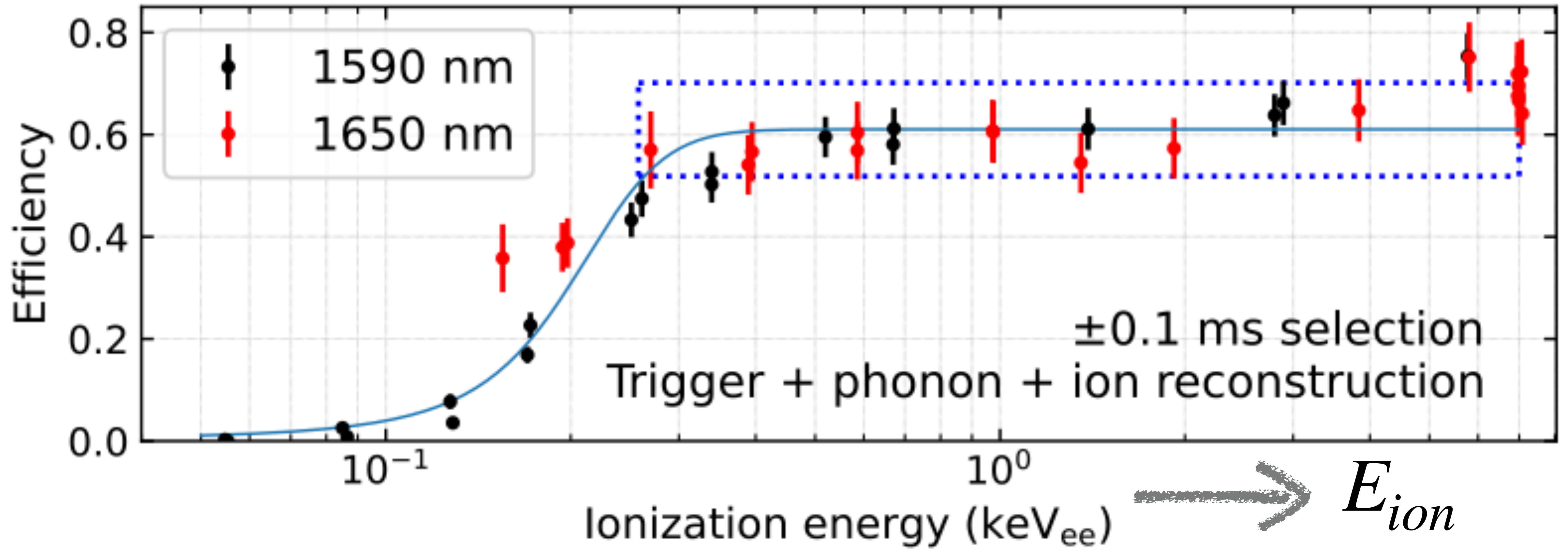

→ E_{ion}

RUN014 →

Feb. 2024 | Apr. 2024 | May 2024 | Oct. 2024 | Jan. 2025 | Jun. 2025 | Jul. 2025

Background levels

155 h of reactor ON

253 h of reactor OFF and ^{252}Cf neutron source

Muon veto coincidences removed

Electron recoil band

Nuclear recoil (NR) band

Heat-only events

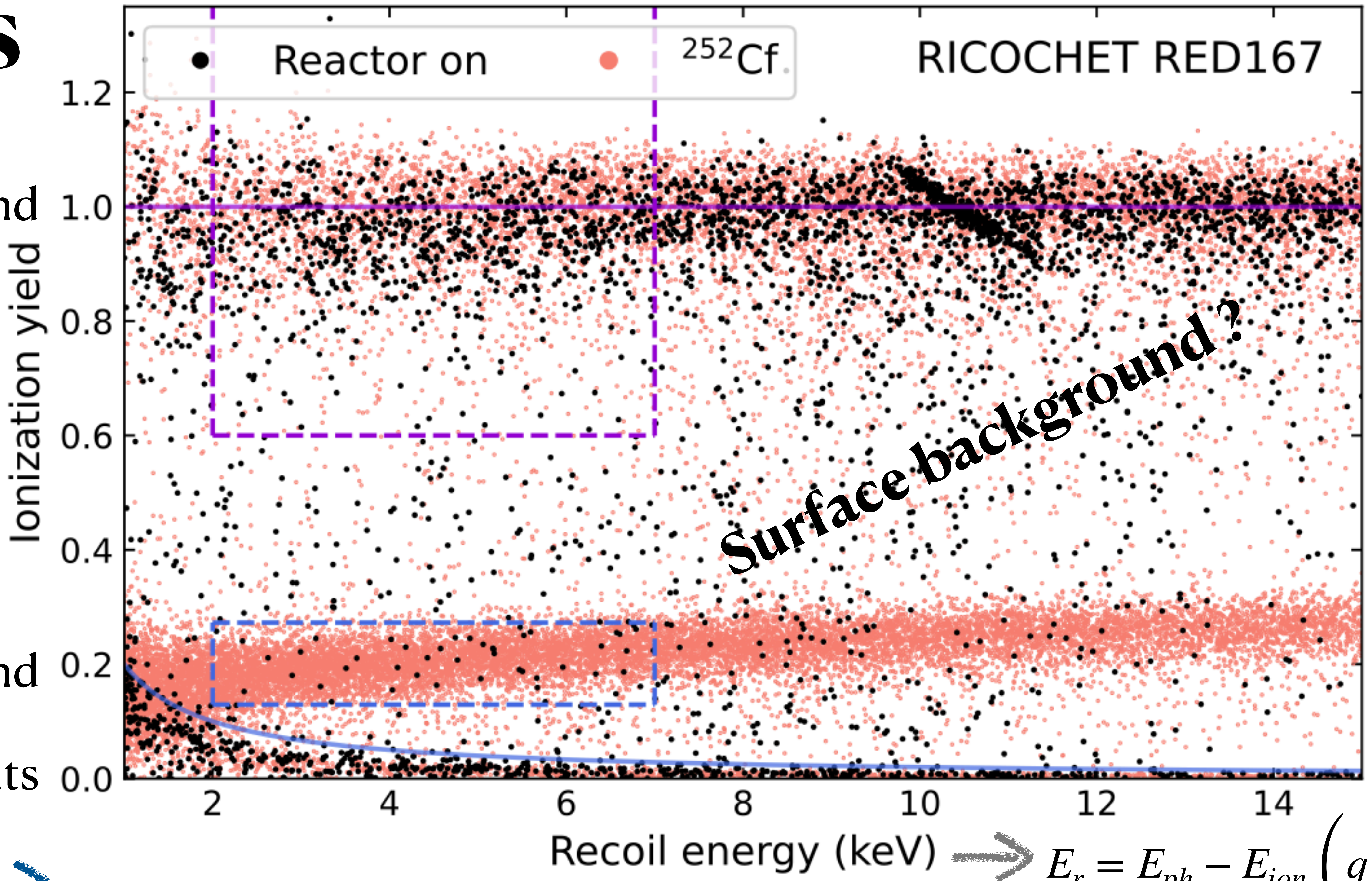

$E_r = E_{ph} - E_{ion}\left(q\frac{V}{\epsilon}\right)$

RUN014

Feb. 2024 | Apr. 2024 | May 2024 | Oct. 2024 | Jan. 2025 | Jun. 2025 | Jul. 2025

Background levels

155 h of reactor ON

253 h of reactor OFF and ^{252}Cf neutron source

Muon veto coincidences removed

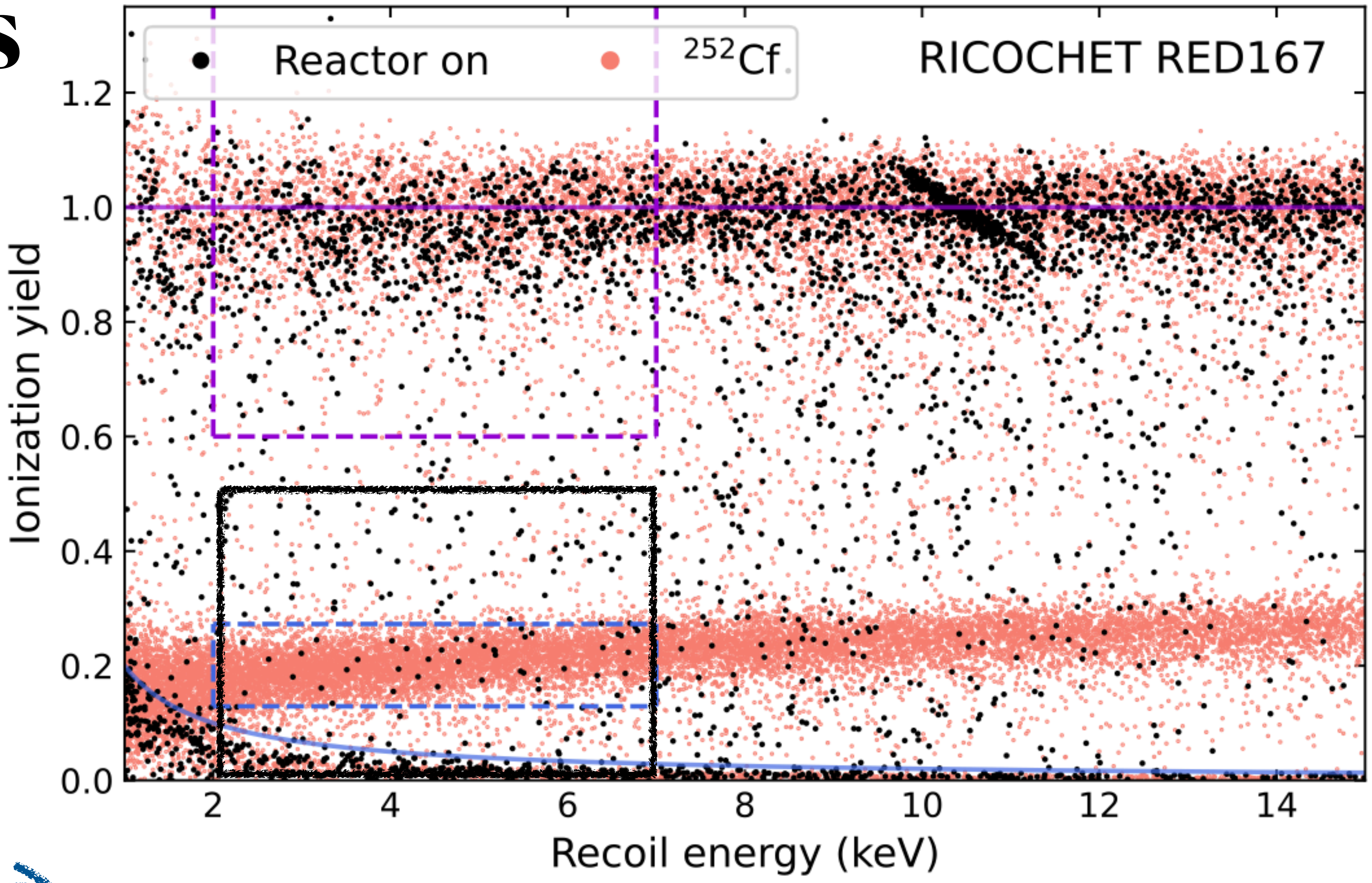

RUN014

Feb. 2024 | Apr. 2024 | May 2024 | Oct. 2024 | Jan. 2025 | Jun. 2025 | Jul. 2025

A. Armatol *et al.*, arXiv:2507.22751 (2025)

Background levels

253 h of reactor OFF and ^{252}Cf source

Muon veto coincidences removed

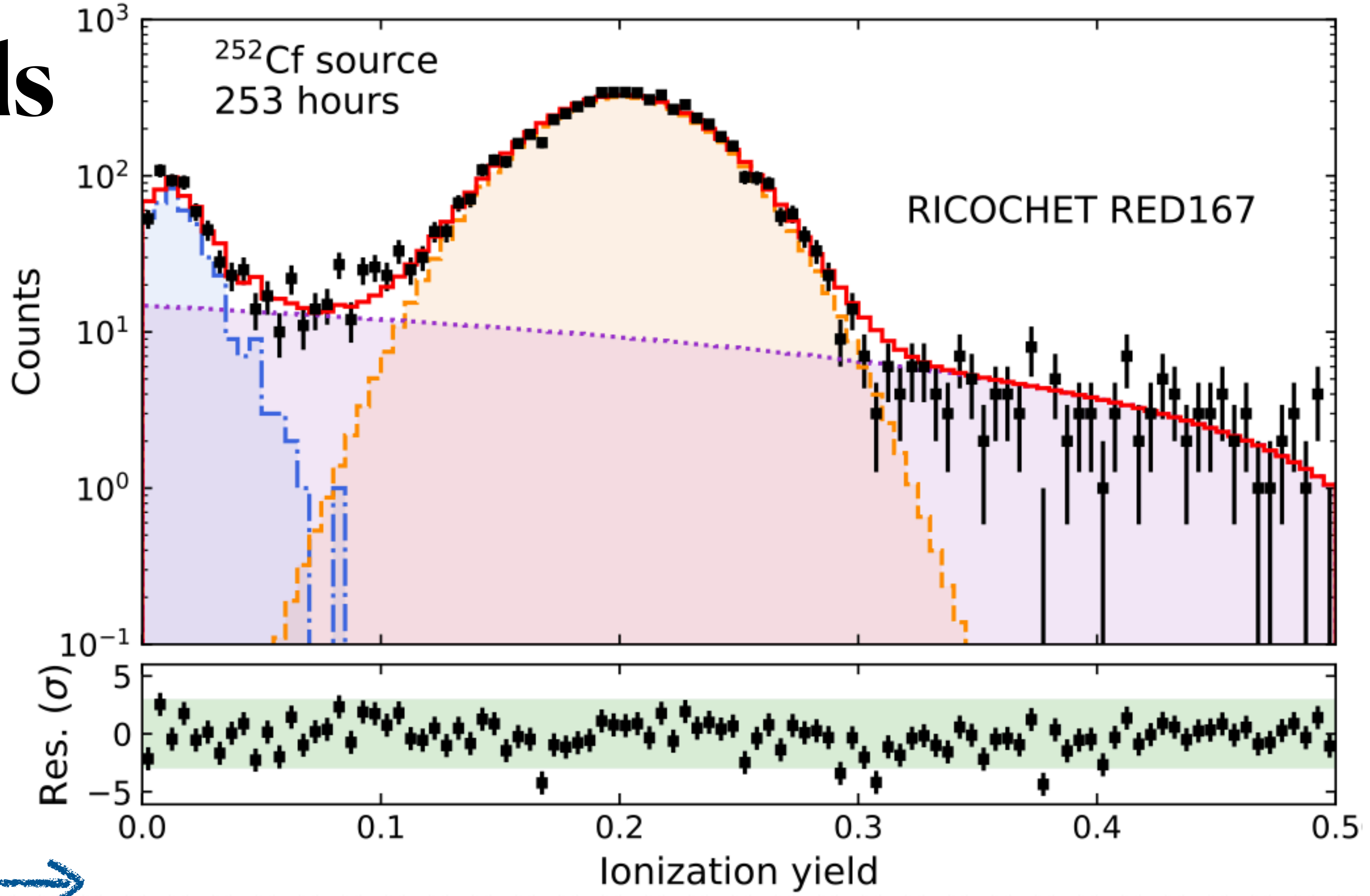

DRU = counts / (kg d keV)

Nuclear recoil rate between 2 and 7 keV

Expected 4.6(8) DRU from cosmogenic and 0.4(1) DRU from reactogenic simulations

DRU = counts / (kg d keV)

Nuclear recoil rate between 2 and 7 keV

Det 1 - NR μ coincidence = 14(3) DRU

Det 2 - NR μ coincidence = 13(3) DRU

Expected 15(2) DRU from cosmogenic simulations

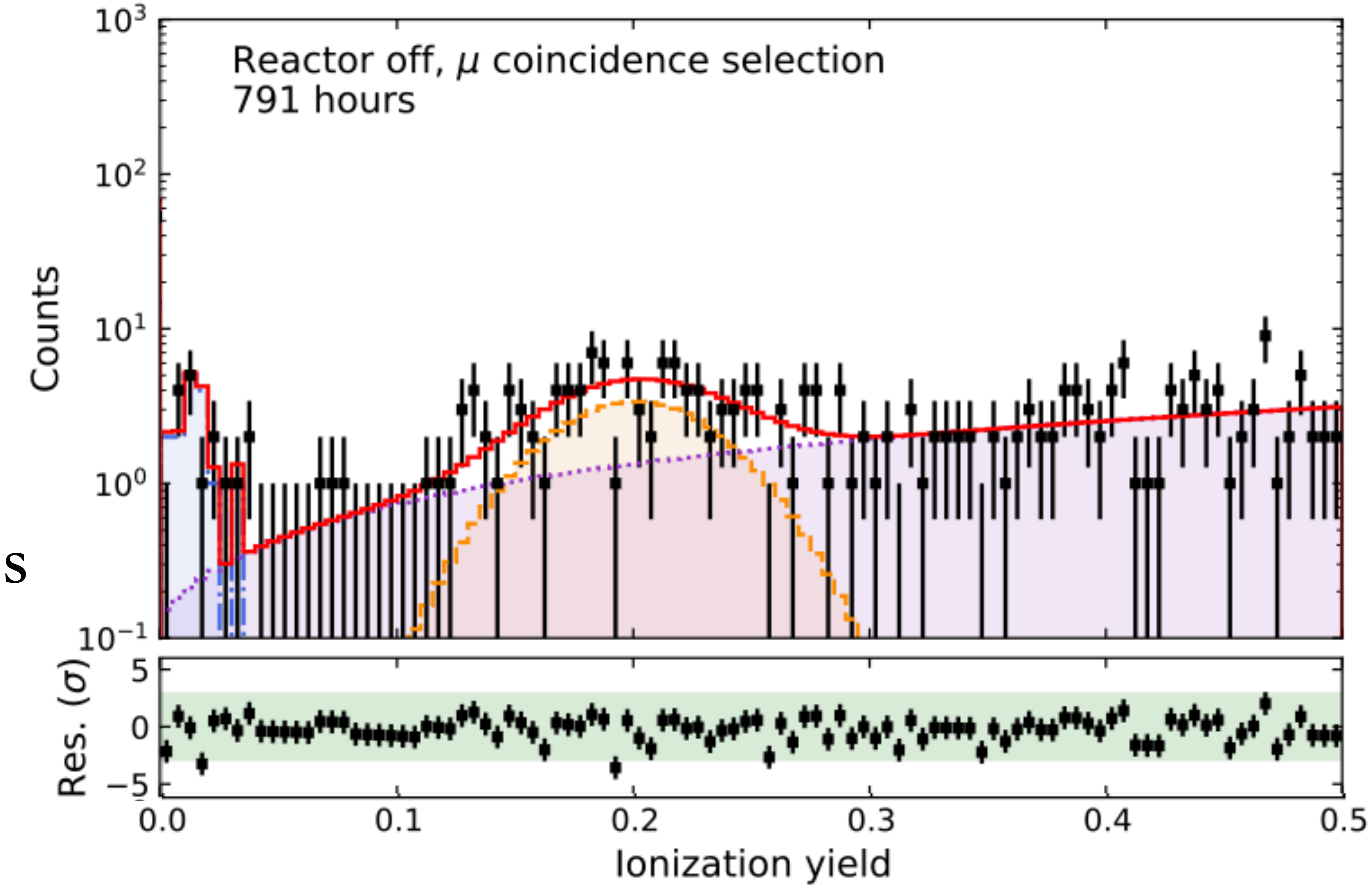

Excellent agreement between the μ coincident data and the cosmogenic simulations

Commissioning

- Payload with nine detectors:
  - 5 with planar geometry
  - 4 with FID geometry → Surface sensitivity
- Cryogenic muon veto installed (for part of RUN015)

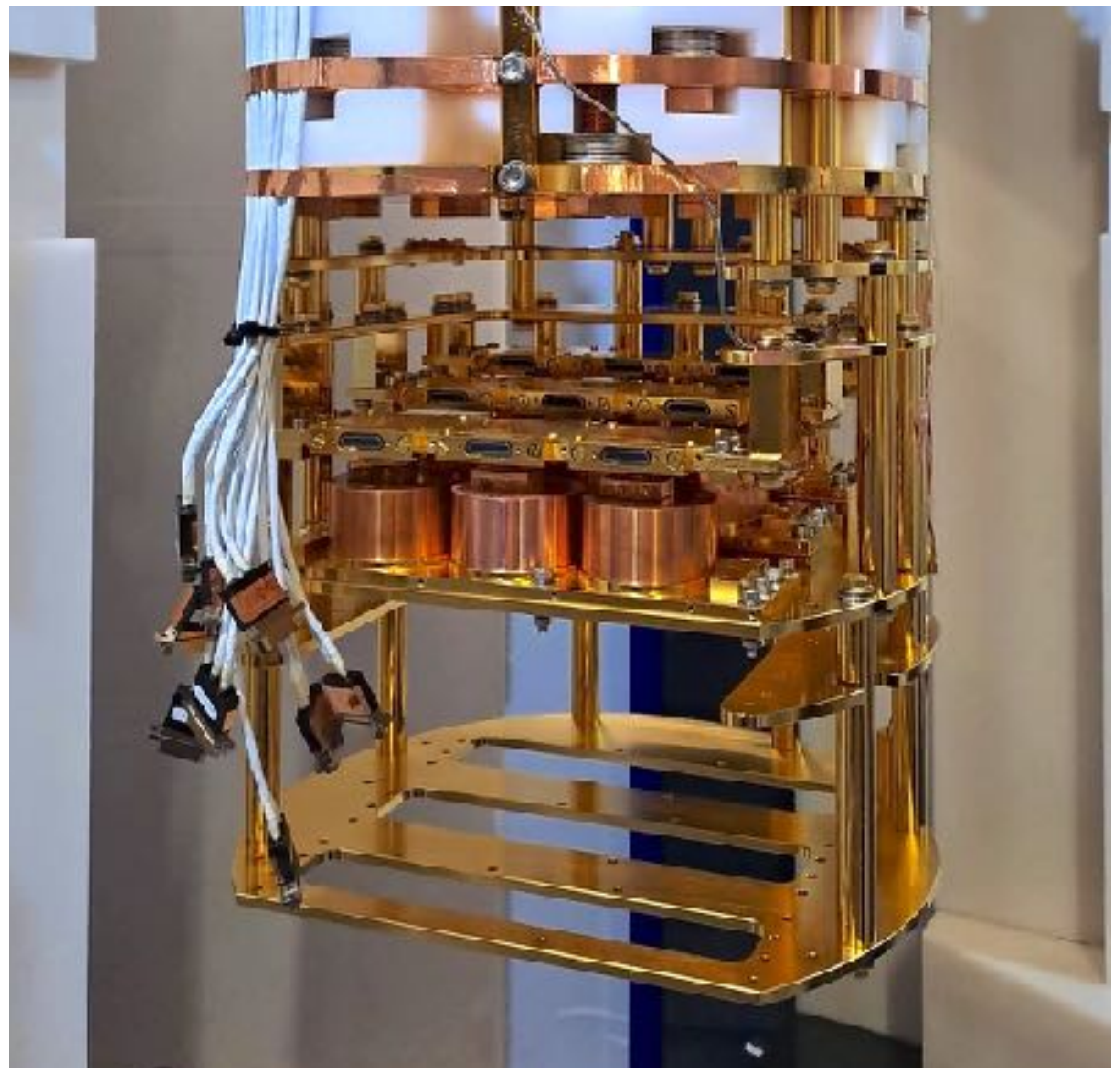

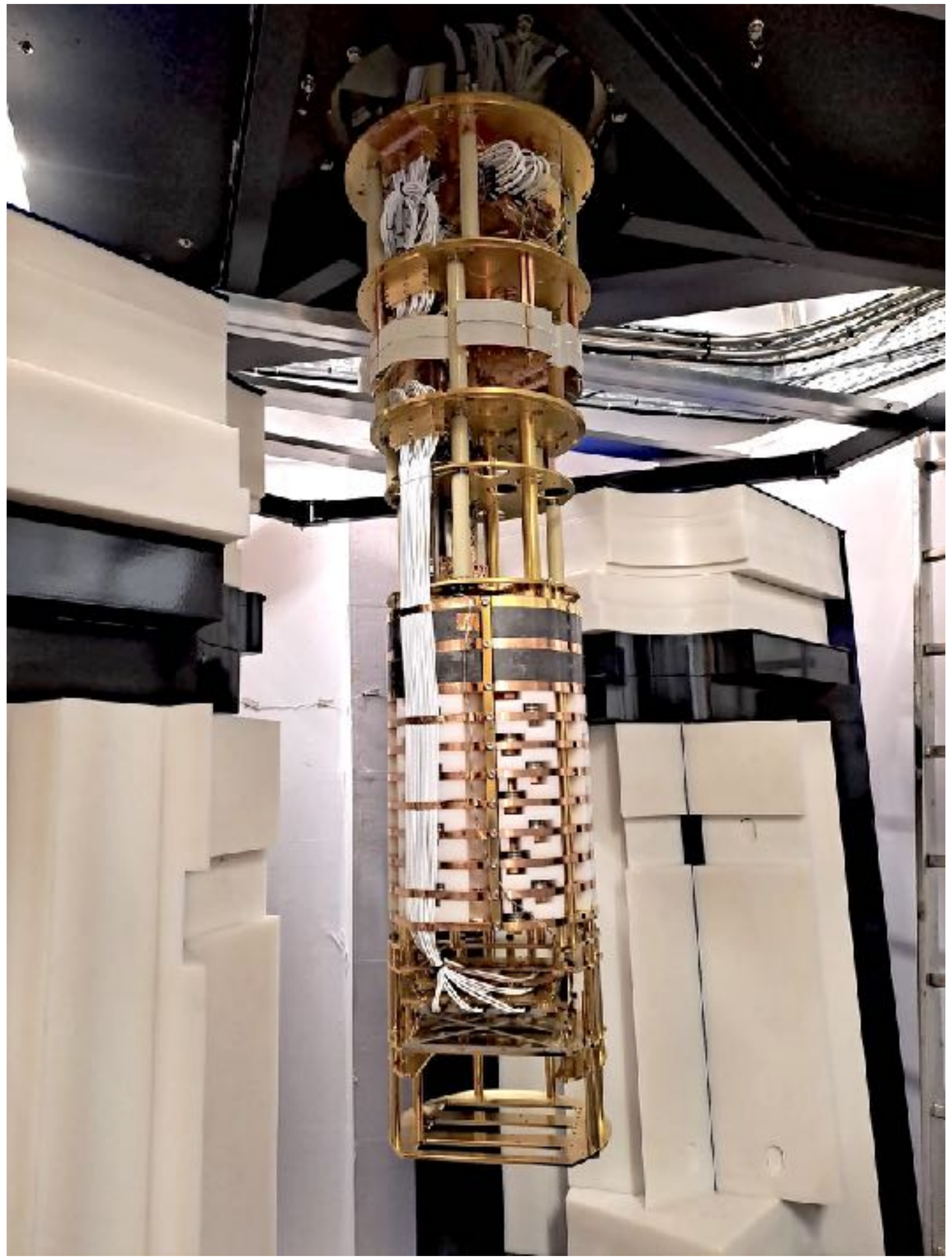

RUN015 →

Feb. 2024 | Apr. 2024 | May 2024 | Oct. 2024 | Jan. 2025 | Jun. 2025 | Jul. 2025

Surface background mitigation

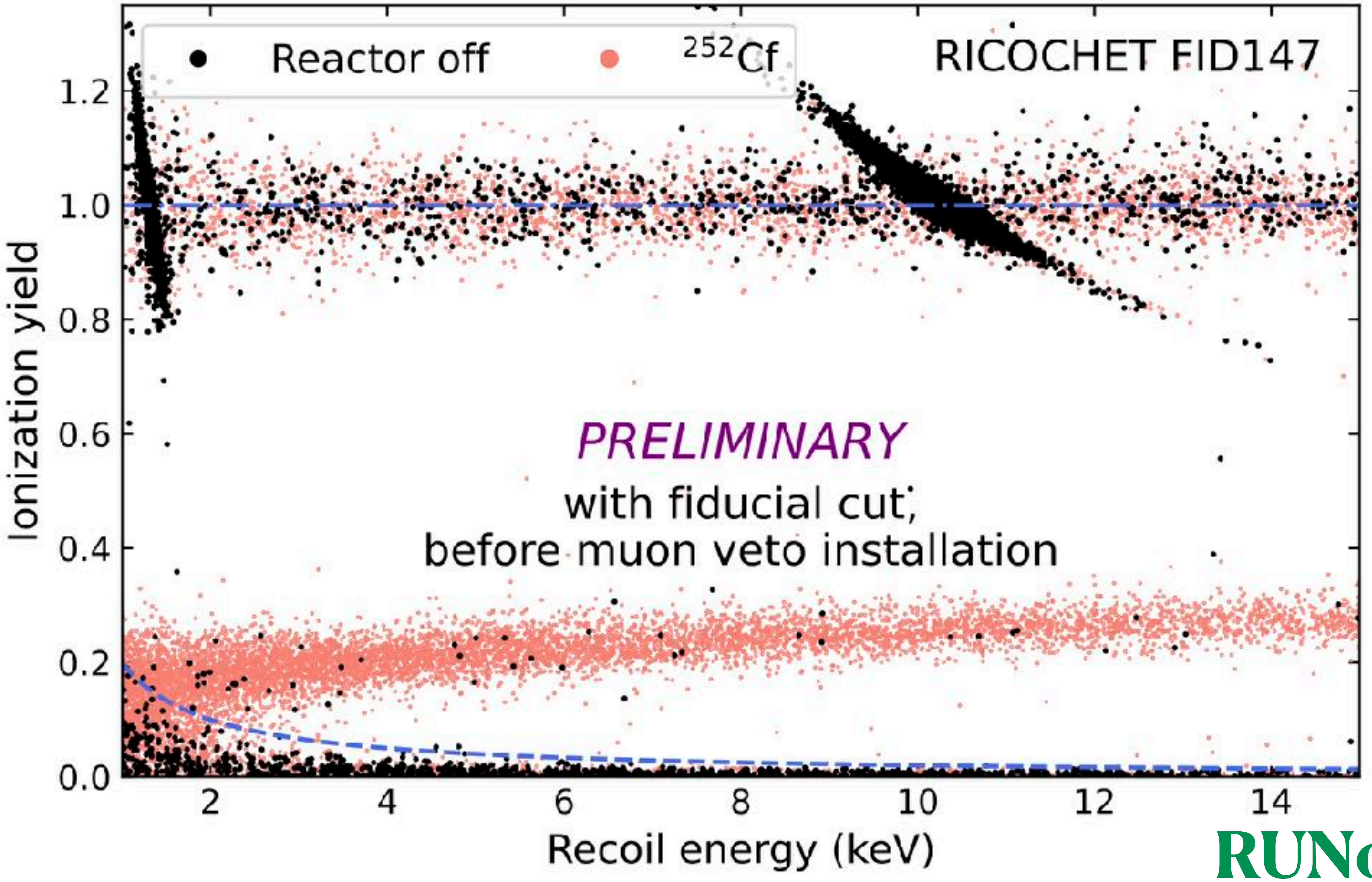

- 277 h of reactor OFF
- 102 h of reactor OFF and ^{252}Cf source
- Without muon veto

- FID detectors with surface rejection capabilities
- Investigation of etching for planar detector holder (in RUN016)

Analysis ongoing...

RUN015

Feb. 2024 | Apr. 2024 | May 2024 | Oct. 2024 | Jan. 2025 | Jun. 2025 | Jul. 2025

Science phase

7 planar detectors
11 FID detectors

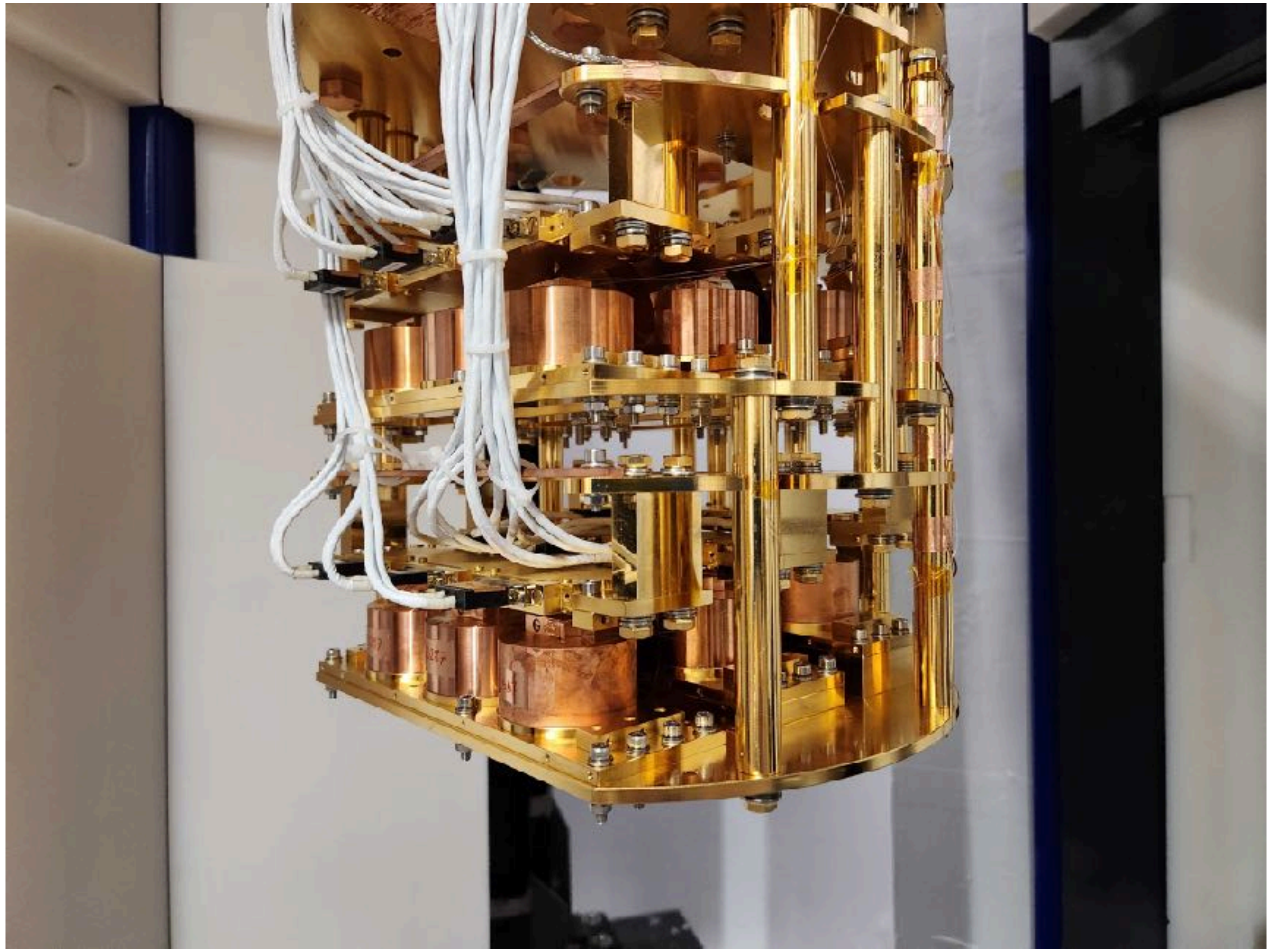

The first science run with the full Ricochet payload (18 detectors for a total germanium mass of 0.76 kg) started in July 2025

New results coming soon !

RUN016

Feb. 2024 | Apr. 2024 | May 2024 | Oct. 2024 | Jan. 2025 | Jun. 2025 | Jul. 2025

Conclusions and outlook

- The installation and phased commissioning are completed.
  - an ionization baseline resolution of σ = 40 eV_{ee} and a phonon baseline resolution of σ = 50 eV_{ph} - 80 eV_{ph} were achieved at the end of RUN014;
  - Backgrounds were measured in RUN014 and an unexpected surface background was identified: mitigation through the use of FID detectors and improved cleaning procedure of the surfaces close to planar detectors.
  - Excellent agreement between the cosmogenic simulations and μ coincident data
- Data analysis of 9 detectors from RUN015 is ongoing…
- **Science phase with the full payload of 0.76 kg of germanium started this July!**

Stay tuned !